Fall 12-2-2022

Interlayered Thin Film Composite (iTFC) Membranes: The Synthesis and Assembly of Active Layer from Conjugated Microporous Polymer

Febby Andini
University of Nebraska-Lincoln, fandini2@huskers.unl.edu

INTERLAYERED THIN FILM COMPOSITE (iTFC) MEMBRANES: THE SYNTHESIS AND ASSEMBLY OF ACTIVE LAYER FROM CONJUGATED MICROPOROUS POLYMER

By

Febby Ekamukti Andini

A THESIS

Presented to Faculty of

The Graduate College at the University of Nebraska

In Partial Fulfillment of the Requirements

For the Degree of Master of Science

Major: Environmental Engineering

Under the Supervision of Professor Siamak Nejati

Lincoln, Nebraska

November 2022

INTERLAYERED THIN FILM COMPOSITE (iTFC) MEMBRANE: THE SYNTHESIS AND ASSEMBLY OF ACTIVE LAYER FROM CONJUGATED MICROPOROUS POLYMER

Febby Ekamukti Andini, M.S.

University of Nebraska, 2022

Advisor: Siamak Nejati

The pursuit of advanced materials with well-defined structures at sub-1 nm size, multi-functionalities, and superior chemical stability is essential for enhanced separation performance but technically challenging. Limitations of conventional TFC membranes for use in Organic Solvent Nanofiltration (OSN) can be addressed by manipulating the pore size and chemical properties of the film with novel materials. Conjugated microporous polymers (CMPs) are promising in a few years because of their highly ordered structure and excellent stability. Porphyrin, one of the basic building blocks, can form a conjugated polymer. Herein, poly(5,10,15,20-tetrakis(4-aminophenyl)porphyrin) or PTAPP, is considerably selected as an active layer from CMPs using an electrochemical approach with various processing parameters such as scan rate, monomer concentration, and cycle number. The assembly of electropolymerized PTAPP membranes with or without an interlayer was studied.

The highest separation performance of PTAPP/Nylon membrane using the dense bottom film as the upper layer of the membrane, accounting for 59% of RB-5 dye rejection in methanol and 7.82 $L.m^{-2}.h^{-1}.bar^{-1}$ methanol permeance. In addition, PTAPP/PE exhibited molecular-sieving selectivity against the mixture of CR and MB dyes and the mixture of CR and MO dyes, with rejection values of 94.48% and 96.16%, respectively. In addition, due to its rigid framework structure of the bottom film, PTAPP/Nylon membrane performed higher NaCl rejection (89%) than the control membrane (53%). Based on SEM characterization, the morphology of poly-TAPP film using MXene as an interlayer revealed the highly porous PTAPP film. However, the pore uniformity, structure, and thickness vary, not strongly correlated with the scan rates.

Key words: *CMP-based film, MXene interlayer, Porphyrin, Membrane Filtration*

ACKWNOWLEDGMENTS

First and foremost, I would like to show great appreciation to my supervisory committee membranes, Dr. Siamak Nejati, Dr. Tian Zhang, and Dr. Bruce Dvorak, for their endless support, encouragement, and guidance throughout my master's studies.

I would like to thank my TCIL colleagues, especially Syed Ibrahim Gnani Peer Mohamed and Christopher Merkel, for always being supportive and helpful while I was going through the challenging experimental works in membrane studies.

Many thanks to the faculty and staff in the Department of Chemical and Biomolecular Engineering and the Department of Civil and Environmental Engineering at the University of Nebraska-Lincoln. Special thanks to my lovely friend, Nicole Church, who just passed away in October. She was the one who always cared for and cheered me up when I was down going through campus life. Without you, I would not be able to stand up myself.

I am also thankful to Fulbright for giving me opportunity to reach my dream of pursuing master’s degree in environmental engineering and for giving me a wonderful experience as an international student in the University of Nebraska-Lincoln, United States.

I would dedicate my accomplishments to my parents in heaven; they are always being the inspirations and reasons for me to not give up on education. The last but not least, I would like to specially thank my husband for putting up with me for all ups and downs in life I went through together with you during my studies. I am so grateful for having you by my side.

TABLE OF CONTENT

LIST OF FIGURES

LIST OF TABLES

CHAPTER ONE: INTRODUCTION

Population growth and industrial expansion have led to high demand for fresh and potable water. Unfortunately, water adequacy is becoming scarce because the available technology is limited to manage a wide range of raw water quality. Among various approaches to treating contaminated water, membrane-based technology became attractive due to its low energy consumption compared to alternative technologies. In membrane filtration, instead of the granular media bed used in conventional filtration, a thin polymeric material is used as a filter media. The inert material of the semipermeable membrane allows fluid to pass through the tiny pores. Thus, it strains the undesired constituents physiochemically at the membrane surface.

1.1 Membrane Separation Classification

Membranes can be viewed as selective barrier which separates the feed stream into two streams known as permeate and retentate as shown in **Figure 1.1**. The permeate is a fluid that passes though the membrane while the retentate is the fluid that does not pass though the membrane and contains the retained particles/ions.

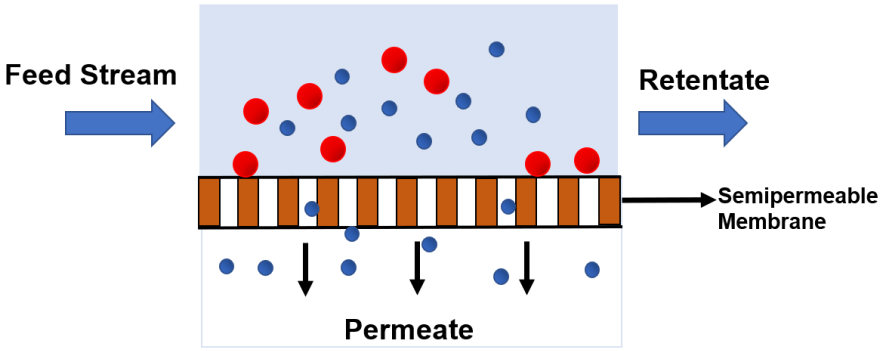

Figure 1.1. Schematic separation process through semipermeable membrane

The separation at molecular and ionic levels is the cut-off for membrane technologies. In this range and separation domain, when the active layer in the membrane is non-porous, the process is driven mainly by solution diffusion. Thus, overcoming osmotic pressure is required, and the process becomes pressure driven. In contrast, if the media is porous and molecular

sieving is taking place, diffusion and flow in the pores can explain the permeation process. The hierarchy of the membrane separation system is presented in **Figure 1.2**. Note that the pores in Reverse Osmosis (RO) membranes are in the range of Angstrom, and these media are not considered porous, but for the sake of simplicity on the chart, the pore size range is given.

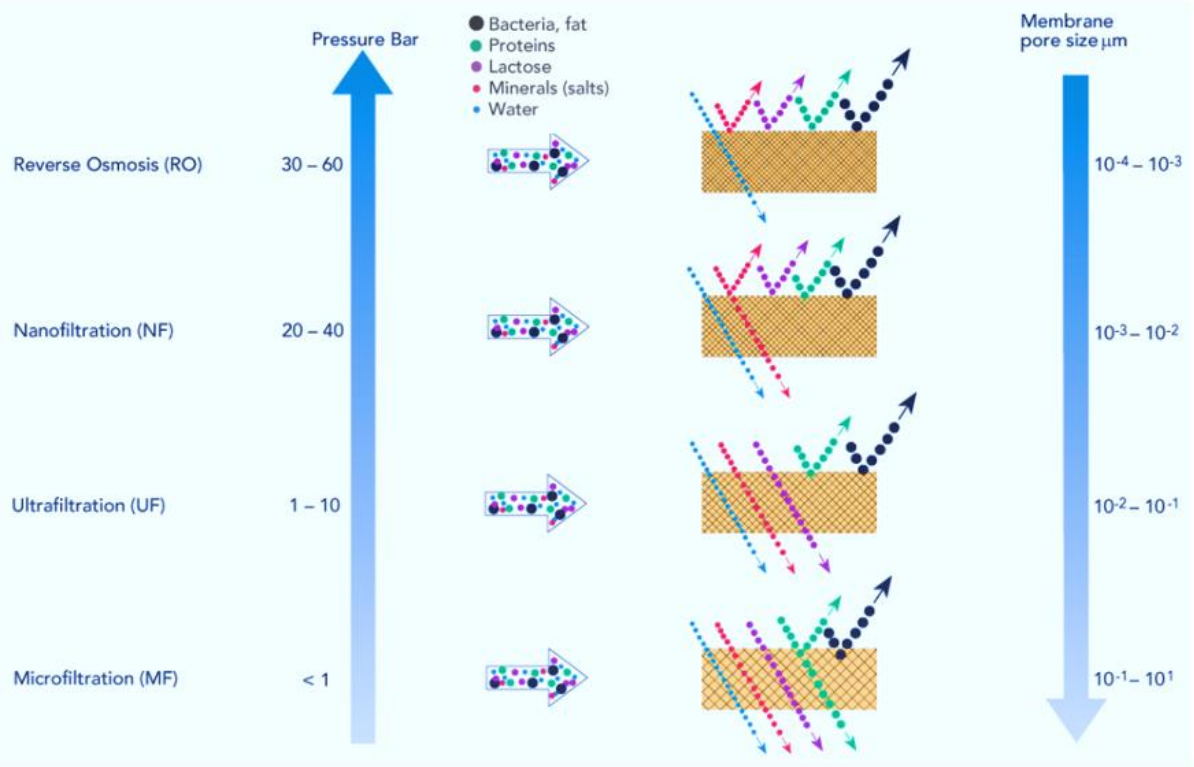

Figure 1.2. Hierarchical pressure driven membrane processes, adapted from Bylund (1995)

Selectivity degree is determined by the relationship of the pore and particle size targeted. There are four membrane processes based on the particle size they separate: Microfiltration (MF), Ultrafiltration (UF), Nanofiltration (NF) and Reverse Osmosis (RO). Microfiltration is effective for removing particulate matters and microorganisms. Ultrafiltration completely separates not only microorganisms but also macromolecules such as protein produced by microorganisms. However, microfiltration and ultrafiltration characterized by loose pores are not practical for salt separation.

Nanofiltration membranes are commonly carried out in the process of demineralization, dye removal, and desalination. They can reject divalent ions such as calcium ions ($Ca^{2+)}$ and magnesium ions ($Mg^{2+)}$ but pass monovalent ions such as sodium ions (Na+) and potassium ions (K^{+}). Due to its distinctive ability in separation, nanofiltration is a more considerable technology in terms of effectiveness, feasibility, and economy. RO membranes are widely used in water purification and desalination. This membrane is slightly different from other membranes because the driving force is influenced by two essential properties: pressure and solute concentration through diffusion.

1.2 Motivation of Study

Nowadays, many industries driving the manufacture of pharmaceuticals, oils, and chemicals produce waste solvents; hence, solvent separation by membrane technology is necessary. Organic solvent nanofiltration (OSN) is an emerging technology that has encouraging efficiency with respect to the energy input, but it is commonly used to separate or purify organic solvents. OSN membranes with chemical resistance and precise molecular weight cut-off are currently pushed across the boundaries for molecular sieving in a wide range. Opposed to the existing membrane separations by molecular size through nanopores, separation by OSN membrane relies heavily on the perm-selectivity occurring in selective materials. However, the OSN membrane is plagued by the presence of inherent non-uniform pores, limiting the pathway for permeant flowing through (Lu et al., 2021).

Over the years, OSN technologies employed an integrally skinned asymmetric membrane known as a thin-film composite (TFC). TFC membrane comprises an ultra-thin polyamide(PA) layer, mass-produced on a mesoporous substrate via interfacial polymerization (IP). Polyamide (PA) is synthesized at the interface of the two immiscible phases using the Schotten-Baumann reaction (Yan et al., 2016; Istirokhatun et al., 2022). IP technique is the most accepted approach for PA-TFC membrane fabrication, supported by independently optimized properties of either PA or porous support layer. However, poorly controlled polymerization during the synthesis may cause heterogenous pores and defects in PA film, degenerating the molecular sieving ability. Moreover, TFC-based-OSN membrane is also challenged by the exposure to harsh conditions such as organic solvent, which seriously weakens membrane stability. Therefore, the solvent permeance and rejection against the targeted solutes are not well-maintained simultaneously.

The pursuit of advanced materials with well-defined structures at sub-1 nm size precision and high fidelity are crucial for organic solvent-stable nanofiltration membranes (Zhang et al., 2022) but is technically challenging. The limitation of conventional TFC membranes for use in OSN can be addressed by manipulating the pore size and chemical properties of the film with novel materials. Various progressive efforts have been made to upgrade TFC membrane by integrating crystalline porous organic materials such as framework materials (metal-organic frameworks and covalent organic frameworks) (Dey et al., 2017; Rajasree, Li, and Deria, 2021) and conjugated microporous polymer (CMPs) (Zhou et al., 2020; Zhou et al., 2021; Lu et al., 2022) into membranes. These materials can be fine-tuned at nanoscales, allowing the formation of a selective layer with tunable pores and excellent chemical stability.

Among the class of porous organic materials, CMPs have been increasingly studied for fast molecular separation because of their enormous rigidity and permanent microporosity. Zhou et al. (2021) suggested that CMPs-based membrane revealed ion-sieving enhancement with homogeneity in sub-nanometer pores and tunable membrane thickness. CMPs displayed not

only a well-structured microporosity for strengthening molecular sieving but also insolubility under harsh synthesis conditions such as high temperature and pressure, desirable for continuous fabrication (Li et al., 2021). The highly ordered nanostructured rendered by CMPs permits tailored selectivity and permeability for OSN. Zhang et al., 2022). However, their mechanical strength possibly drops under pressure-driven conditions. Then, the enhancement of CMPs film was performed by Lu et al (2022) using electrochemical approach, providing robust structure and excellent stability in dimethylformamide (DMF) solutions at pressure up to 30 psi. Simultaneously, scalable, defect-free materials under industrial conditions are encouraged with CMPs fabricated using electrochemical approach (Lu et al., 2022).

Conjugated polymer structures such as pore uniformity, are largely mirrored by building block or monomer structures with high chemistry. A wise choice of molecular building block provides directional bonding to prevent the porous structure from collapsing (Zhou et al., 2021). Several reported building blocks for CMPs-based film are 1,3,5-tris(N-carbazolyl) benzene (TCB), 2,2',7,7'-tetra(carbazol-9-yl)-9,9'-spirobifluorene, and tris(4-carbazoyl-9-ylphenyl)amine (TCTA) (Zhang et al., 2022; Zhou et al., 2020; Lu et al., 2022). The rarely explored monomers from organic material, called porphyrin, were investigated as building blocks. One example of porphyrin derivatives is tetra(4-aminophenyl)porphyrin (TAPP) and that was used to generate polymer films (Walter and Wamser, 2010). However, poly-TAPP film has not yet been explored for aqueous separations. Using TAPP as specific building blocks for CMPs provides the highly interconnected nanofibrous network that features many nanopores, making this film more possible for sized-dependent selectivity and permeability.

.

1.3 Polymeric Organic Material

The degree of selectivity correlates with structural polymeric membranes: non-porous and porous organic material. Thin film composite nanofiltration employs non-porous membranes, characterized by low flux because a densely thin active layer is supported by a loosely support

layer. In the search for membrane to perform high permeability, the pore structure must be accessible to guest molecule across by creating an interconnected network of channels.

Porous organic materials have drawn a great deal of attention in diverse areas, including separation, filtration, catalysis, and gas storage. Strong covalent linkage between various organic building blocks with different geometries and topologies (Zhang et al. 2020) builds a multi-dimensional porous network that features with superior inherent porosity, excellent stability, pre-designable and tunable structure. The most advantage of porous organic material in separation is an ability to possess hierarchical pores across multiple length scales (Liu and Liu, 2020) with precise control as well as interconnectivity, which is beneficial for achieving sized-dependent permeability and selectivity for solute targets.

1.4 Family of Porous Organic Materials

Triggered by the high demand for separation at the molecular and ionic levels, the exploration of porous materials into membranes is increasingly intensive in research. The most breakthrough materials in the class of porous materials are the porous organic frameworks, including covalent organic frameworks (COFs) and metal-organic frameworks (MOFs), covalent organic polymers (COPs), and conjugated microporous polymers (CMPs). Each member has imperative attributes, as discussed in the following sub-sections.

1.4.1 Covalent Organic Frameworks (COFs)

First documented by Yaghi and co-workers in 2005, numerous COFs with different topology have been identified. Nowadays, the various COFs including boroxine-linked, boronate ester-linked, imine-linked, hydrazone-linked, azine-linked, ketoenamine-linked, triazine-linked imine-linked, phenazine-linked, and sp^2-carbon linked COFs were reported. Their extended structures vary based on rigid organic building blocks, which contain elements such as C, N, O, B, and S. By linking organic building blocks via covalent bonds, COFs possess a crystalline two-dimensional (2D) or three-dimensional (3D) network structure.

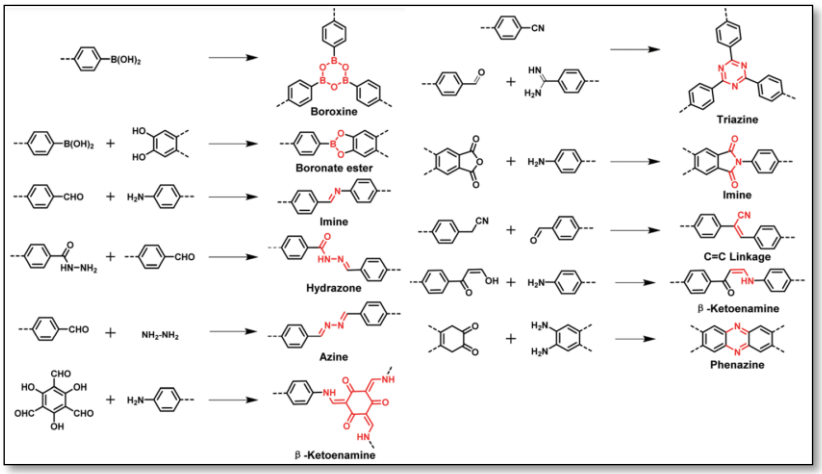

Figure 1.3. *The Classic reactions used for construction of COFs, adapted from Wang et al. (2020)*

Covalent organic frameworks (COFs), an emerging class of material, are distinguished from other polymers because of their crystallinity with highly ordered networks. Their unique properties, such as well-defined crystalline structures, low density, large surface area, tunable pore size, and facilely tailored functionalities (Meng and Mirica, 2021), have made COFs material extremely attractive for the fields of gas adsorption, and storage, separation, catalysis, sensing, drug delivery, optoelectronic, and energy storage. Among them, the membrane-based separation by COFs material based on molecular sieving is superior, thanks to COFs structural features, especially homogenous pore size and ordered pore channel. In OSN application, the appropriate pore size inside the frameworks allows the solvent molecules to pass through without compromising the damage to the COFs structure (Li et al., 2019).

Granted with periodic, ordered, and extended skeletons, functional building blocks are precisely integrated (Zhang, et al., 2020). The arrangement of specific functional sites on the organic building block using the design principle of reticular chemistry determines the functionality of COFs. Thus, the chemistry of linking molecular building blocks via strong bonds is defined by reticular chemistry to achieve the extended crystalline structures. Additionally, through inefficient molecular packing, the tuned porosity is procured, and the component

molecules which have concavities can form an interconnected grid, for instance COF-5, originated from molecular building blocks as shown in **Figure 1.4**.

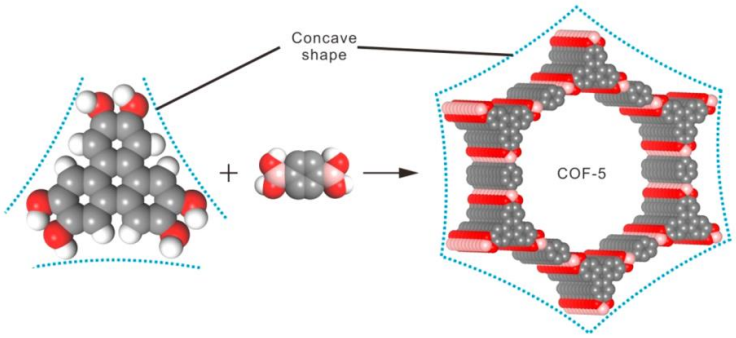

Figure 1.4. *Structural model of COF-5 formed from molecular building blocks. Carbon, boron, and oxygen atoms are colored gray, pink, and red, respectively. Hydrogen atoms are excluded for clarity, adapted from Das et al. (2016)*

1.4.2 Metal Organic Frameworks (MOFs)

The solid material with linked discrete metal cluster was found by Hoskins and Robson in 1990, and its term was officially pronounced in 1995 as metal organic frameworks (MOFs). Among all porous materials, MOFs, a sister material of COFs, is rapidly emerging in separation applications with high fidelity and high flux (Michael et al., 2016). Similar to COFs, MOFs are acknowledged for their high porosity, tunable pores, and distinctive chemical functionalities. The uniqueness of MOFs material is the desirable structures and frameworks compositions achieved by employing various metal ions and organic ligands. Their longer organic linkers and larger metal cluster demonstrates higher porosity and larger pore size, in comparison to the zeolites. The frameworks of MOFs are constructed by interconnecting organic linkers with metal nodes or secondary building blocks (SBU) through strong metal-carboxyl coordination (Rajasree, Li, and Deria, 2021). Hence, the organic ligands act struts, while the metal centers are called an inorganic SBU that serves as the joints in MOFs frameworks. Expanded by reticular chemistry, the replacement of the struts or node with another of comparable symmetry permits tailored functionalities in wide range.

1.4.3 Covalent Organic Polymers (COPs)

Covalent Organic Polymer (COPs), commonly built by COFs, inherits the highly crosslinked porous structure, functionality, and exceptional sieving characteristics. COPs, decorated by incorporating multiple functionalities into a single framework, can successfully obtain a distinct length and geometry of building blocks, leading to finely tuned porosity in broader range. Lightweight elements such as C, H, N, O, F, and S form the backbones of COPs (Skorjanc, Shetty, and Valan, 2021). Characterized by the extended covalent bonds, COPs are encouraging material for membrane because they are insoluble in organic solvents. Moreover, their stability and non-complex fabrication procedures have gained widespread attention in the areas of storage, separation, and catalysis.

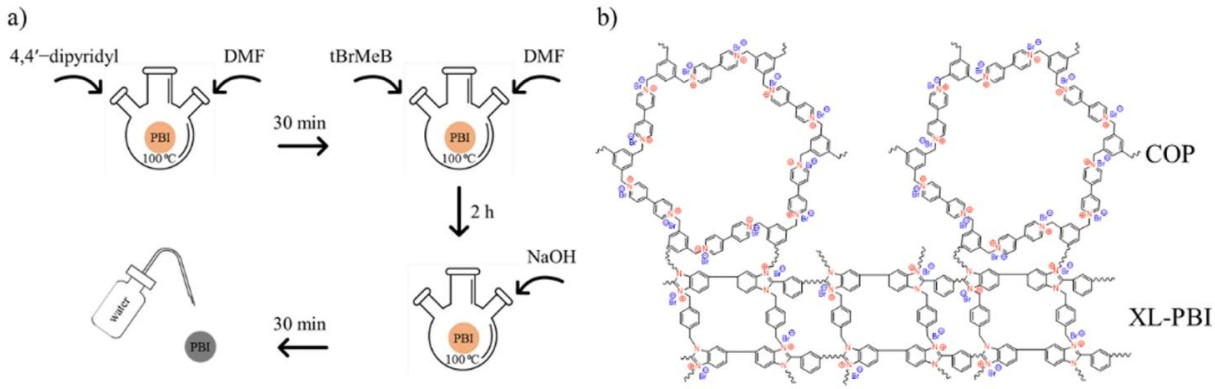

Figure 1.5. *(a) Schematic Procedure of COP membrane preparation (b) chemical structure of composite Membrane with COPs, adapted from Tashvigh and Benes (2022)*

1.4.4 Conjugated Microporous Polymers (CMPs)

Conjugated microporous polymers are a sub-class of porous organic polymers (POPs) classified as amorphous polymers. CMPs were first introduced in 2007 by using Sonogashira-Hagihara palladium coupling to link aromatic halides to aromatic alkynes, which are recently known as poly(aryleneethynylene) (PAE) networks (Das et al.,2017). This amorphous nature of CMPs is contributed by the freedom of rotation about the S bonds formed between building blocks, allowing the structure to be disordered and having a broader pore size range. Like

crystalline porous polymers such as COFs, CMPs pore size is associated with the monomer strut length, but it is more statistical. More importantly, CMPs possess extended π-conjugated composition, which originates from a microporous network (multiple carbon-carbon bonds or aromatic rings) that builds a building block within the system (Dawson, Cooper, and Adam, 2012; Xiang et al. 2015). Alternating single and multiple bonds arising from the overlap of two p orbitals (or d orbitals) crosswise with an intermediary σ-bond (Muller, 1994), result in conjugation to a certain degree. The significance of the extended π-conjugated skeleton and excellent porosity endows the CMPs material as a potential candidate for molecular sieving (Lu et al., 2022)

1.5 Goals and Objectives

The main goal of this work is to establish the advanced material that offers a precise tailored pore, multi-functionalities, superior chemical stability for enhanced separation performance in challenging environment as well as offers the simplification of processing that potentially revolutionizes its applicability in industry. The objective is to investigate the novel selective layer material, a porphyrin containing CMPs for TFC membrane combined with innovative assembly method using MXene interlayer that conducts electricity. Porphyrin-based film, particularly poly(5,10,15,20-tetrakis(4-aminophenyl)porphyrin) or PTAPP, is considerably selected and subsequently prepared with different sets of electrochemical parameters and transferred on various supports for testing and characterization. The separation performance of the bare and modified membranes in terms of permeability and selectivity under different conditions is studied.

1.6 Organization of the Thesis

The first chapter of this thesis is the introduction. The goal of the introduction is to provide an overview of the state of art polyamide layer in thin film composite nanofiltration membrane including the merit and demerit in industrial applications, and to acknowledge the porous material and its classification that represents the functionality. Chapter 2 is a review of the

literature that is related to the nature of porphyrin and its role as a building block, electropolymerization, and the role of interlayer for enhanced separation performance. Chapter 3 includes the materials and methods in the preparation, fabrication, testing, and characterization of porphyrin-based membrane. Chapter 4 includes result and analysis of regarding to permeability, selectivity degree, and scalability of the prepared membranes with various parameters.

CHAPTER TWO: LITERATURE REVIEW

2.1 Porphyrin Based-Membrane

Porphyrins exist commonly in natural environments, and they play a crucial role in mechanism (Chen, Zhu, and Kaskel, 2021). Chlorophyll in green plants, for instance, is one structure that utilizes porphyrin. Photosynthesis needs a complex, particularly magnesium, which is provided by porphyrin. Then, in conjugated double bonds of molecules of chlorophyll, π - electrons attribute to the absorptions of the photons.

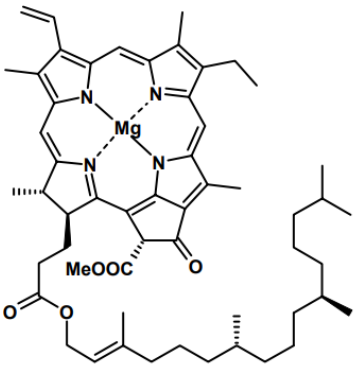

(a)

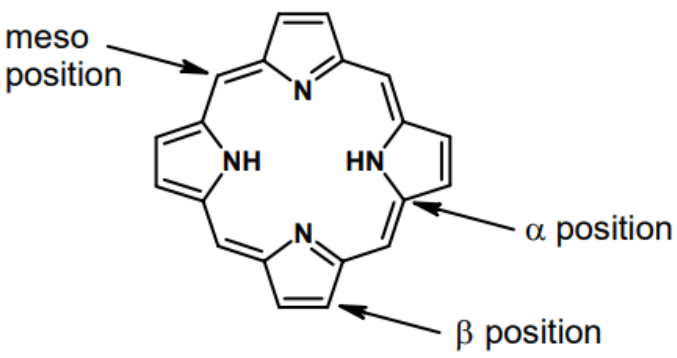

(b)

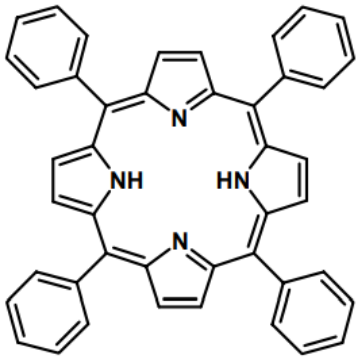

(c)

Figure 2.1. *a) chlorophyll, b) porphin – the modest form of porphyrin, and c) meso-tetraphenylporphyrin*

Besides the naturally synthesized porphyrins, synthetic porphyrins have been introduced by adopting the structure of their parent, called porphin ($C_{20}H_{14}N_4$). The first synthesis of Porphyrin is tetraphenylporphyrin (TPP), done by Rothmund in 1936 using benzaldehyde and pyrrole. The conceptual construction of synthetic porphyrin is generally macromolecular heterocyclic substituted by various functional groups at the *meso*-position or *β*-position (Gottfried, 2020). Due to their size, they are ideal to be bound to desired chemical groups (e.g., metal ions).

Porphyrin derivative, known as poly(5,10,15,20-tetrakis(4-aminophenyl) porphyrin) or PTAPP was introduced by Walter and Wamser (2010) in the form of film. PTAPP inherits rigid and robust structures, unlocalized π-electrons, functionality, high surface area, and the ability to coordinate with transition metals along with structural adjustability. In this regard, porphyrin has attracted the special attention of most practitioners in numerous scientific works such as gas storage and separation, catalysis, energy storage, and photocatalysis.

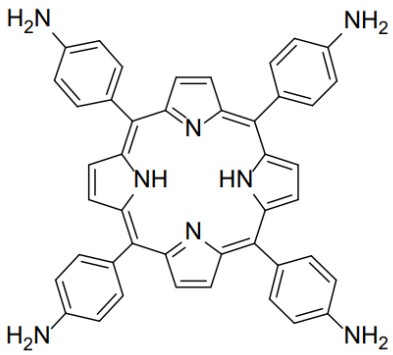

Figure 2.2. *PTAPP structure*

2.2 Electrochemical Polymerization

Having deficiencies of thin film preparation and assembly that involves further processing, the method that has more simplicity and reproducibility but still offers the desirable polymeric properties is highly required. In recent years, the formation of thin polymer films with equivalent porous surface can be generated by electrochemical polymerization (Cando, Enriquez, Tausch, and Scherf, 2019). In this method, the working electrode is immersed in an

electrochemical cell containing a monomer, a doping agent, and the electrolyte solution while the potential is applied to the working electrode. While the monomer is chemically oxidized, free radicals are formed, then they initiate the polymerization rate. Thus, the polymer film is directly deposited onto the electrode surface (Fomo et al., 2019; Lu, Lie, Wang, and Zhang, 2022).

The essential feature of EP is the well-defined thickness and formation process of the film by controlling the electrochemical parameters, such as redox scan mode and the number of cycles. Moreover, the size of the film area can be adjustable depending on the WE surface size. Therefore, EP is a straightforward, practical approach for fabricating polymer films or membranes.

The application of the EP method for making homogenous porous films in the field of membrane separation has arisen in numerous studies. In the context of porphyrin polymer film, the polymerization of TAPP via EP was previously done by Walter and Wamser (2010). The forming radical cation of TAPP, then subsequently followed by a series of coupling reactions between the oxidized para-aminophenyl substituents, induces polymerization. The morphology of electrochemically fabricated poly-TAPP (PTAPP) film is a highly interconnected nanofibrous network. In other porous organic materials, conjugated microporous polymers (CMPs) film was successfully fabricated via EP process (Zhou et al., 2020), leading to robust structure, superior mechanical strength and ductility, high surface area, and uniform pore size of 1 nm. A relevant study has been reported by Lu's group (2022), forming a rigid cross-linked structure of CMPs membrane from tris(4-carbozoyl-9-ylphenyl)amine (TCTA) through EP process for organic solvent nanofiltration, with carbon nanotubes (CNTs) pre-deposited on a substrate as the conductivity booster.

2.3 Interlayer Thin-Film Composite (iTFC)

The progressive efforts to break the restraint of the permeability-selectivity trade-off have focused on the triple-layered thin-film composite, consisting of nanomaterials or a coating layer sandwiched between the support and selective layer. Katulla et al. (2015) introduced a gutter layer in three-layer composite membranes. The defect-free thin selective layer is successfully fabricated if the gutter layer material is compatible with the selective layer. The polyamide film is grown after coating layers or nanomaterials pre-deposited on the porous substrate. Various nanomaterials have been reported for fabricating interlayered thin film composite membranes, including titanium oxide (TiO_2), and carbon nanotubes (CNT), while the interfacial coating materials include polydopamine (PDA), polyphenols, and polyelectrolytes.

Unlike conventional composite membranes, the novel TFC mediated by interlayer is structurally constructed based on hierarchical sizes (Xue, et al. 2022). In other words, the interlayer is prepared for a highly permeable thin film composite, in which the dense pore of interlayer material is always higher than the active layer but lower than the substrate pores. The benefit of the interlayer is the tuning interfacial polymerization (IP), responsible for the morphology of the polyamide selective layer in TFC, leading to optimized transport paths inside poorly permeable selective layer as well as enhanced permeance without altering the selectivity performance (Dai et al., 2022, Gong et al., 2020). As reported by Karan et al. (2015), the introduction of cadmium hydroxide as a sacrificial layer for preparing thin-composite membrane gains control over the IP reaction, then the flux is increased by two orders of magnitudes, superior to commercial membranes.

The effect of the interlayer is continuously studied with different materials in later years. PDA-coated substrate conducted on the formation of polyamide thin film composite nanofiltration revealed the enhanced water permeance of approximately one order magnitude and high rejection towards multivalent salts (Yang et al., 2020). PDA interlayer plays multiple roles in the shortening of water transport pathways, the prevention of intrusions by polyamide into the

substrate pores, the formation of nanovoids within separating layers, and the acceleration of cross-linking (Yang et al., 2020).

A similar study featuring a multilayered-TFC membrane, the role of an interlayer was attributed to MXene, intercalated with carbon nanotubes, exhibiting a water flux four times higher than the commercial TFC. (Sun et al., 2021). The significance of the CNT interlayer in the TFC-NF membrane was proven to tailor the pore structures (e.g., pore size and thickness), then greatly increased the permeance accompanied by nearly 100% of salt/dye rejection (Gong et al. 2019). Additionally, the interlayer of the framework, ZIF-8, into the PA-TFC membrane showed a smoother surface and more negatively charged, which are ideal conditions for forming a thin, loose, and defect-free PA film. The as-prepared interlayered TFC membrane with framework endowed the relatively stable rejection, but its permeance is twice that of the pristine one (Zhao et al., 2021).

2.4 Highlight of Research

Of all works of literature given, this study investigates the novel thin-film composite assembled as a multilayered membrane, highlighting the porphyrin as a novel separating layer via electrochemistry. MXene material has dual functions, an interlayer and a conductive material as support for working electrode surfaces in electropolymerization. In other words, the selective layer and interlayer material, and fabrication method are the newest investigation.

CHAPTER THREE: METHODOLOGY

This chapter presented explicitly the materials and the approaches for porphyrin-based membranes, starting from the synthesis, fabrication, membrane performance evaluation, and characterization. The novel pathway, in-situ bottom-up synthesis, was used to prepare TAPP monomers, and electropolymerization was used to fabricate poly-TAPP film onto different porous supports. In the next section, the prepared membranes were further tested to evaluate separation performance under concentration-driven and pressure-driven. In the last section, the characterization of PTAPP film on the basis of surface morphology and chemical properties was observed.

3.1 Material

All chemicals were bought from Sigma-Aldrich and Acros Organics and were used as received. Some materials such as (5,10,15,20-tetrakis(4-aminophenyl) porphyrin) or TAPP and MXene were self-synthesized in transformative coatings and interfaces laboratory (TCIL), University of Nebraska-Lincoln. Nylon (pore size of 0.2 μm, a diameter of 47 mm), Polyethylene (PE) and Polytetrafluoroethylene (PTFE) (pore size of 0.45 μm, a diameter of 47 mm), and Teflon (HDPE, pore size of 1 μm, a diameter of 47 mm) were purchased from Sterlitech. Indium Tin Chloride (ITO glass) with a size of 50 x 50 mm and 70 x 70 mm, and conductivity of 10 ohm was bought from ebay and washed thoroughly using DI water, acetone, and ethanol before use.

3.2 Synthesis of 5,10,15,20-tetrakis(4-aminophenyl) porphyrin) (TAPP)

In situ bottom-up synthesis of raw material includes two-step synthesis, from TNPP to TAPP monomers, then the crude product is purified using Soxhlet extraction. The detailed procedures are presented in the following sub-sections.

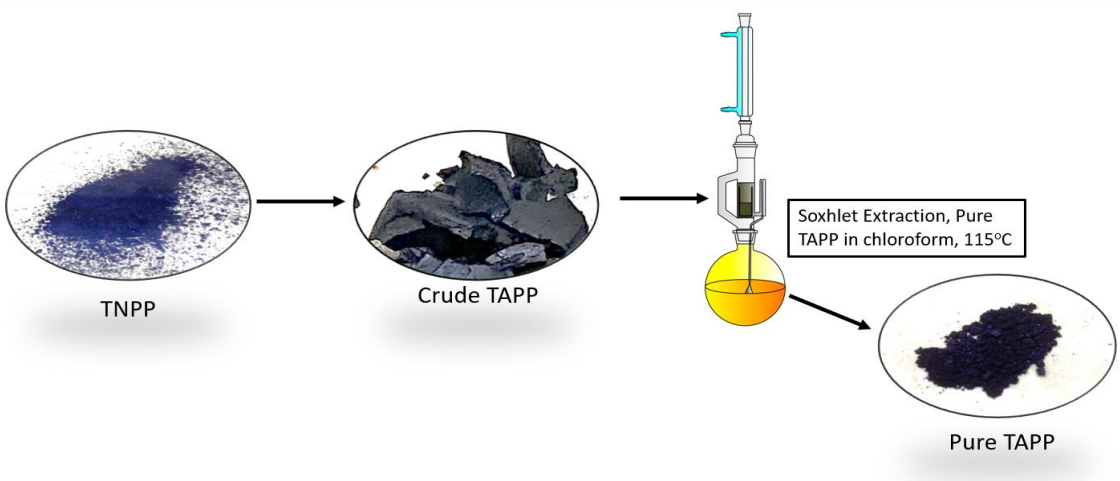

Figure 3.1 *The schematical process of TAPP material preparation*

3.2.1 Synthesis of 5,10,15,20-tetrakis(4-nitrophenyl)porphyrin (TNPP)

A mixture of 50 mL nitrobenzene (Acros Organics, 99%) (50 mL) in 14 mL lactic acid (Alfa Aesar, 98%) was heated up to 135°C for 1.5 hours, under reflux. To this mixture, a premixed solution of nitrobenzene (24 mL), distilled pyrrole (Acros Organics, 99% extra pure) (55 mmol, 3.68 g), and p-nitrobenzaldehyde (Acros Organics, 99%) (55 mmol, 8.00 g) was gradually added over 20 min, 2 mL per instance. The reaction mixture was covered by alumina foil, preventing exposure to light, and stirred at 135 °C for 2.5 hours; the mixture was cooled down to 60 °C, and 30 mL of dry methanol (Sigma-Aldrich, HPLC grade ≥99.9%) was injected into the flask. When the temperature of this mixture reached around 25 - 30°C, the product was separated by vacuum filtration and washed thoroughly with methanol. The purple-like crystalline retentate was dried in a vacuum oven at 60 °C overnight (2.45 g, yield 22.4%).[20] 1 H NMR (300 MHz, CDCl3): δ 8.24 (s, 8H, pyrrole ring), 7.7 (d, J =8.2 Hz, 8H, ArH), 7.65 (d, J = 8.2 Hz, 8H, ArH), -2.71 (s, 2H, pyrrole NH).

3.2.2 Synthesis of (5,10,15,20-tetrakis(4-aminophenyl) porphyrin) (TAPP)

A solution of 2.06 g (2.6 mmol) TNPP in 94 mL concentrated hydrochloric acid (Sigma-Aldrich, ACS reagent, 37%) was prepared and mixed at room temperature under nitrogen (Matheson, extra pure) gas for 30 min. The premixed solution of $SnCl_2.2H_2O$ (Sigma-Aldrich, reagent grade, 98%) (8.75 g, 38.7 mmol) was added dropwise to the TNPP solution. The reaction mixture was stirred under nitrogen for 2.5 hours at room temperature, and then the temperature was increased to 80 °C and stirred for 1 hour. The mixture was cooled down to 0°C in an ice bath, and the residues were filtered. 250 mL DI water was added to the crude product, and pH was adjusted to ~9 using ammonium hydroxide (Sigma-Aldrich, ACS grade, 28-30%). The precipitant was separated by filtration.

3.2.3 Purification of TAPP Crude Product

The crude product of TAPP was further purified using soxhlet extraction. The crude product was put into the extraction thimbles (cellulose, 20 x 80 mm, fisher scientific) while a 100 ml chloroform (Sigma-Aldrich, 99.9%) in a round flask was prepared, and stirred at 115°C for 2 – 3 days. After the extraction is complete, the solvent containing the extracted product, pure TAPP, was removed using buchi rotary evaporator. The remaining pure TAPP in flask was dissolved in a 30 ml hexane (Sigma-Aldrich, 99.9%, then was readily filtrated. The obtained dark blue powder was dried in the vacuum oven at 60°C overnight (1.4 g, yield 81.5%).[20] 1 H NMR (300 MHz, CDCl3): δ 8.9 (s, 8H, pyrrole ring), 7.9 (d, J =8.14 Hz, 8H, ArH), 7.0 (d, J = 8.14 Hz, 8H, ArH), 4.04 (s, 8H, NH2), -2.69 (s, 2H, pyrrole NH).

3.3 Synthesis of MXene

A 3 g Titanium aluminium carbide (Ti_3AlC_2) (200 mesh, ≥99.8% purity, Foesman) was gradually added to a 60 mL Hydrogen Fluoride (HF) (AR, ≥40%, Aladdin), followed by magnetic stirring hermetically for 24 hours at room temperature. Subsequently, the resulting solution was washed by distilled water and centrifuged at 6,000 rpm for 5 minutes, which was repeated several times until the pH of supernatant to nearly 7. A 60 mL of Dimethyl sulfoxide (DMSO) (Sigma-Aldrich, 99.9%) was added and stirred at room temperature for 18 hours. Then, the residual DMSO was moved by centrifugation and distilled water was added. Next, ultrasonication was conducted for 6 hours. Finally, samples were vacuum filtered and dried at room temperature for 24 hours in vacuum oven.

3.4 Membrane Fabrication

This study involves two membrane designs prepared with different process schemes. The first design is a bilayer thin composite membrane in which the electropolymerized PTAPP film is transferred to a porous substrate. Meanwhile, the second design is a triple-layered PTAPP membrane, where PTAPP is electropolymerized in-situ on MXene/Support membrane substrate. The performance of the as-prepared two membranes, regarding the constructed layers, is evaluated.

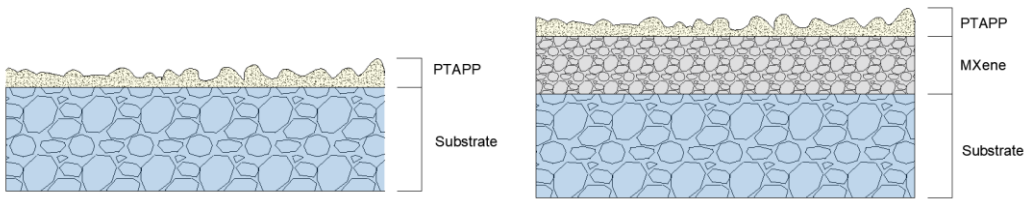

Figure 3.2 *The illustration of (a) bilayer and (b) tri-layer PTAPP membrane*

3.4.1 Bilayer PTAPP Membrane

The first design is a bilayer PTAPP membrane, consisting of a selective PTAPP film and porous support. This process includes three stages: the electropolymerization process which is simultaneously monitored by cyclic voltammetry (CV), free-standing film, and membrane fabrication, as shown in **Figure 3.3**. The detailed procedures are described in sub-sections.

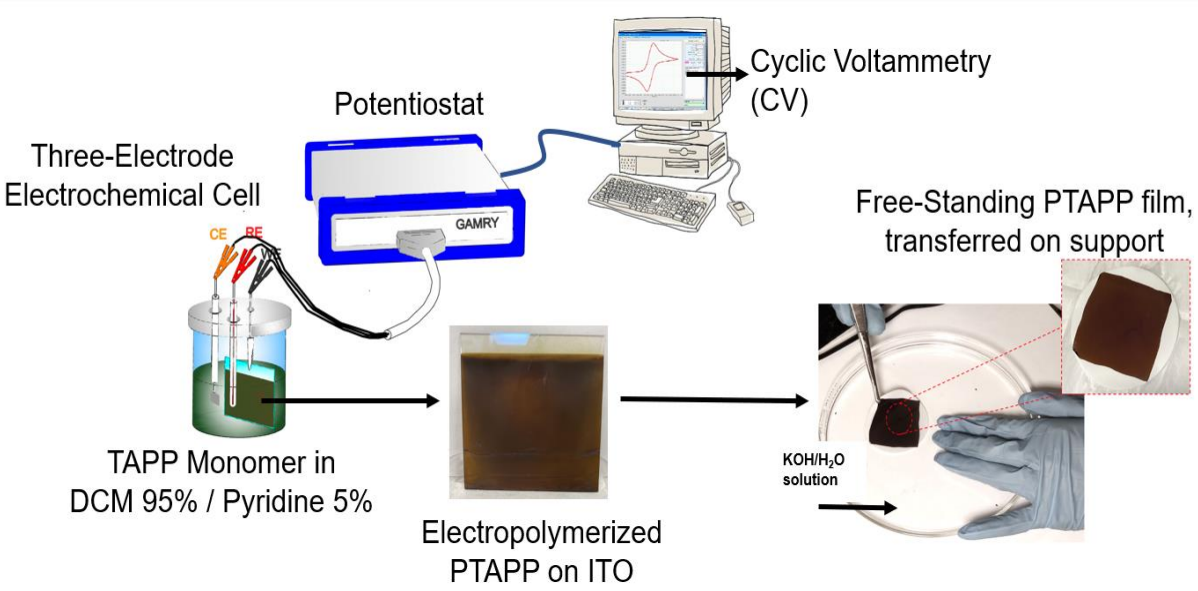

Figure 3.3 *The schematic of PTAPP/Substrate membrane fabrication*

3.4.1.1 Electro polymerization of PTAPP film on ITO

Conductive porphyrinic polymers were carried out in a three-electrode electrochemical cell oxidative polymerization: working electrode (WE), counter electrode (CE), and reference electrode (RE), as shown in **Figure 3.3**. They were kept together and connected to a potentiostat, an electronic device responsible for electrodeposition by producing the maintainable potential; then allowing the current to be drawn into the system with a constant voltage (Fomo et al., 2019). The working electrode is composed of conductive solid material, monomer solution, and the supporting electrolyte, and the intrinsic nature of the WE surface determines the ease of electropolymerization rate. The reference electrode, usually made of silver wire immersed in Ag/AgCl solution, maintains the potential constant at the working

electrode surface. Meanwhile, a counter electrode serves the electricity from the signal source to the working electrode, forming the current circuit. In the EP process, the coupling series between cationic radicals or radical cationic with neutral monomers takes place, which is electrochemically oxidized to initiate the growth of thin film onto the surface of the solid electrode material.

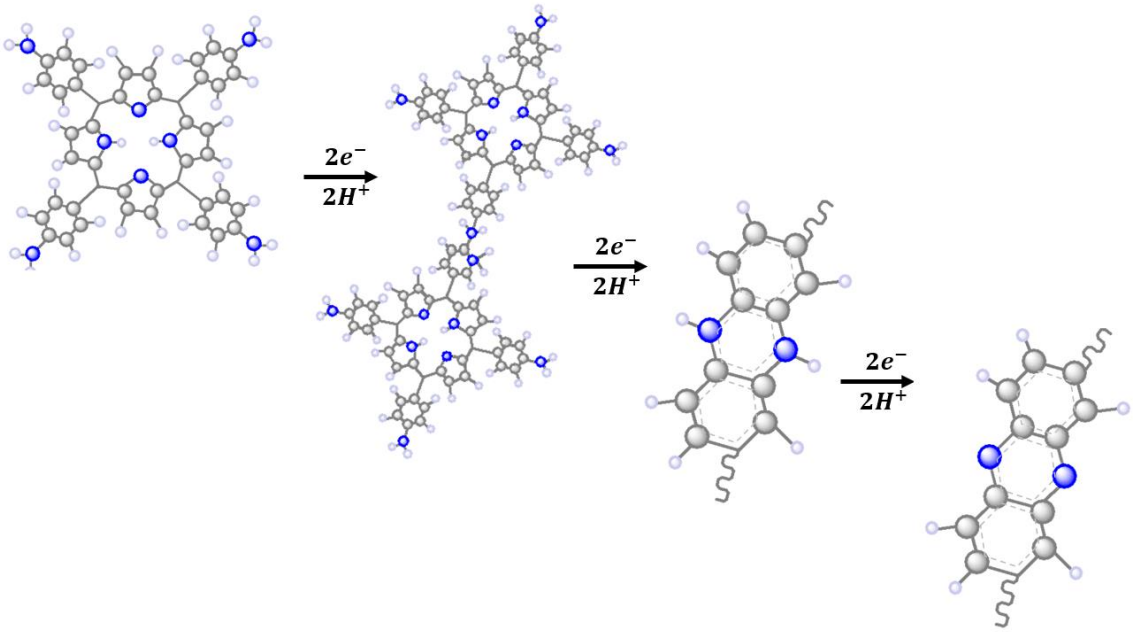

Figure 3.4 *The electropolymerization mechanism of TAPP through amine coupling reactions*

Following its pioneer work (Walter and Wamser, 2010), electropolymerization of PTAPP film was carried out with Indium Tin Oxide (ITO) as the solid working electrode. The conductive side of ITO glass is immersed in a TAPP solution in dichloromethane (DCM) containing 5% v/v pyridine as the co-crystallization agent and 0.05 M tetrabutylammonium hexafluorophosphate (TBAPF6) as the supporting electrolyte. TBAPF6 was purified with the mixture of DI and ethanol (Acros Organic, 99%) ratio of 1:6 before use in the electropolymerization process. $Ag/AgNO_3$ electrode and PT wire were chosen as the reference electrode and counter electrode, respectively.

The physical and chemical properties of the PTAPP films are significantly determined by electrochemical parameters; in this study, they are limited to potential scan rate, and nature and concentration of monomer. The scan rate was set to 5, 10, and 15 mV/s, whereas the

monomer concentration ranged from 0.5 to 1.0 mM. In attempting to explore the surface of the porphyrinic film, this study evaluated the use of copper metal ions substituted into the TAPP monomer. Other parameters, such as the number of cycles, temperature, and volume percentage of addictive pyridine, were kept constant. In addition, the electropolymerized PTAPP film on different sizes of ITO glass material is demonstrated to attend to the need for scalable-designed polymer film in the industry. The electropolymerized PTAPP film on ITO glass was washed using acetonitrile (CH_3CN) to remove unreacted monomers and the remaining supporting electrolyte.

In this study, the oxidative polymerization process of monomers was conducted in the direction of linear sweep on cyclic voltammetry (CV) curve in multiple cycles, in the swept potential range between -0.4 and 0.7 V. The performed CV curve is based on the measurable current at the working electrode during potential scans, and CV is an irreversible reaction of oxidation and reduction. The total current in a system result from the sum of faradic current and charge transfer, , $I_{system} = I_{faradic} + I_{charging}$. The resulting current from charging is proportional to the scan rate, , $\frac{dV}{dt}$. In a given closed circuit, the current flows in that circuit because a number of charges or ion carriers are induced by a potential difference (voltage). As the scan rate increases, more current flows. Higher currents indicate that the diffusion rate is more than the reaction rates, and fewer ions participate in the charge transfer reactions. The cycling of the poly-TAPP film is repeated, up to ten cycles, as shown in **Figure 3.5**.

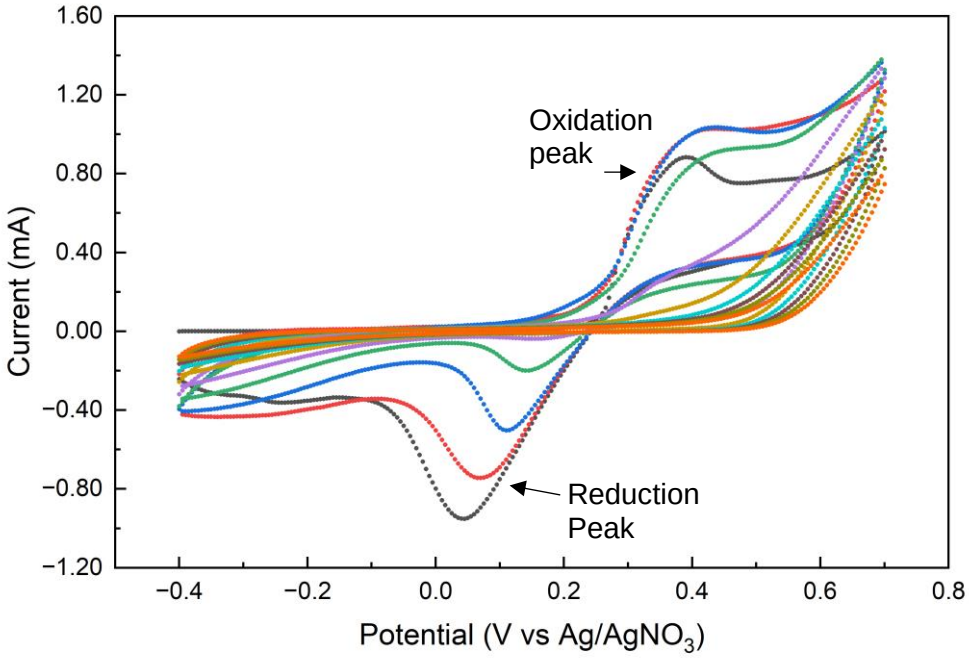

Figure 3.5 *The cyclic voltammogram of TAPP electropolymerization on ITO glass using a scan rate of 5 mV/s at room temperature, performed in 0.5 mM TAPP, 0.05 M TBAPF6, and 5 % v/v pyridine solution*

3.4.1.2 Demonstration of Free-Standing PTAPP Film

Free-standing polymer is a common technique that releases or lift-off the film from its substrate. Interestingly, this method is highly suitable for obtaining large-area films, up to the size of 13 cm diameter with a minimum film thickness (Stadermann et al., 2015). This process works based on the balance of interfacial peeling energy with the swelling-induced strain energy (Freund and Suresh, 2003). When the film and substrate are immersed in a solvent bath, the film is spontaneously induced to delaminate because of swelling by the solvent. Consequently, the film is readily released from the substrate and floats independently on top of the solvent bath.

Since the PTAPP is deposited on ITO glass via electrochemical approach, free-standing film was used to obtain the PTAPP film released from ITO glass substrate with minor potential defects and fractions. As shown in **Figure 3.6**, the electrodeposited film on ITO glass was initially scratched on each side, then immersed in DI water with the addition of a concentrated

potassium hydroxide (KOH, 8 M) solution dropwise. The KOH facilitates the delamination of the thin layer by creating the gap between the ITO glass substrate and PTAPP film. A drop of KOH varies depending on the intrinsic properties of PTAPP film. If the delamination does not happen, the KOH drop is gradually increased. A few drops of ethanol on the top surface of PTAPP film on ITO glass may be necessary if there is no sign of delamination in 30 – 60 minutes.

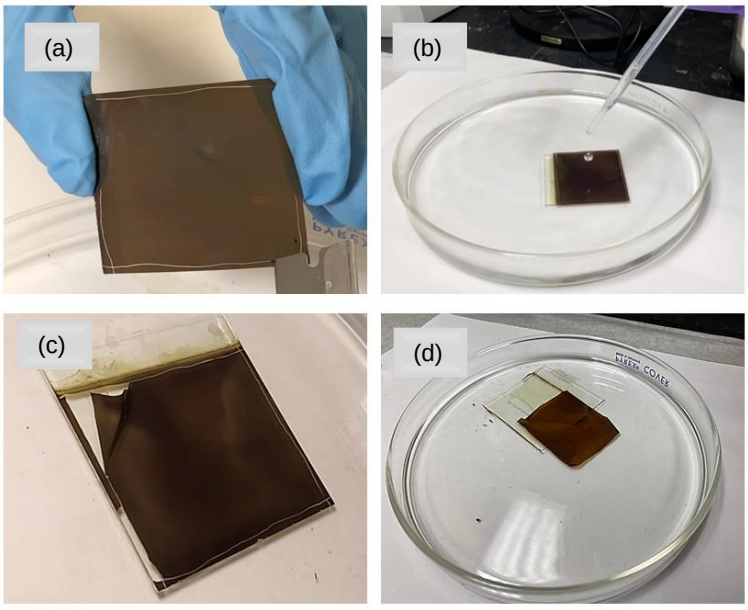

Figure 3.6 *The digital photographic images of free-standing PTAPP film in KOH/H_20 solution, with 8 M KOH, (a) etched PTAPP on ITO, (b) the addition of KOH to DI water, (c) delamination process, and (d) free-standing film*

3.4.1.3 PTAPP/Support Membrane Fabrication

The fabrication of porphyrinic membrane featuring asymmetrical structure is by transferring the freshly free-standing PTAPP film on the porous substrate, as shown in **Figure 3.3**. After transferred, the wet-fabricated membrane was readily used for membrane testing. The size of fabricated membrane depends on the need in the operational unit system. Here, nylon was chosen as the support membrane for dead-end cell while polyethylene (PE) was chosen as the support membrane for static diffusion cell

3.4.2 Tri-layer PTAPP Membrane

The second design is a three-layer PTAPP membrane consisting of PTAPP film, MXene interlayer, and porous support. This process includes MXene membrane fabrication, and electropolymerization of PTAPP film on MXene membrane, as shown in **Figure 3.7**. The detailed procedures are described in sub-sections.

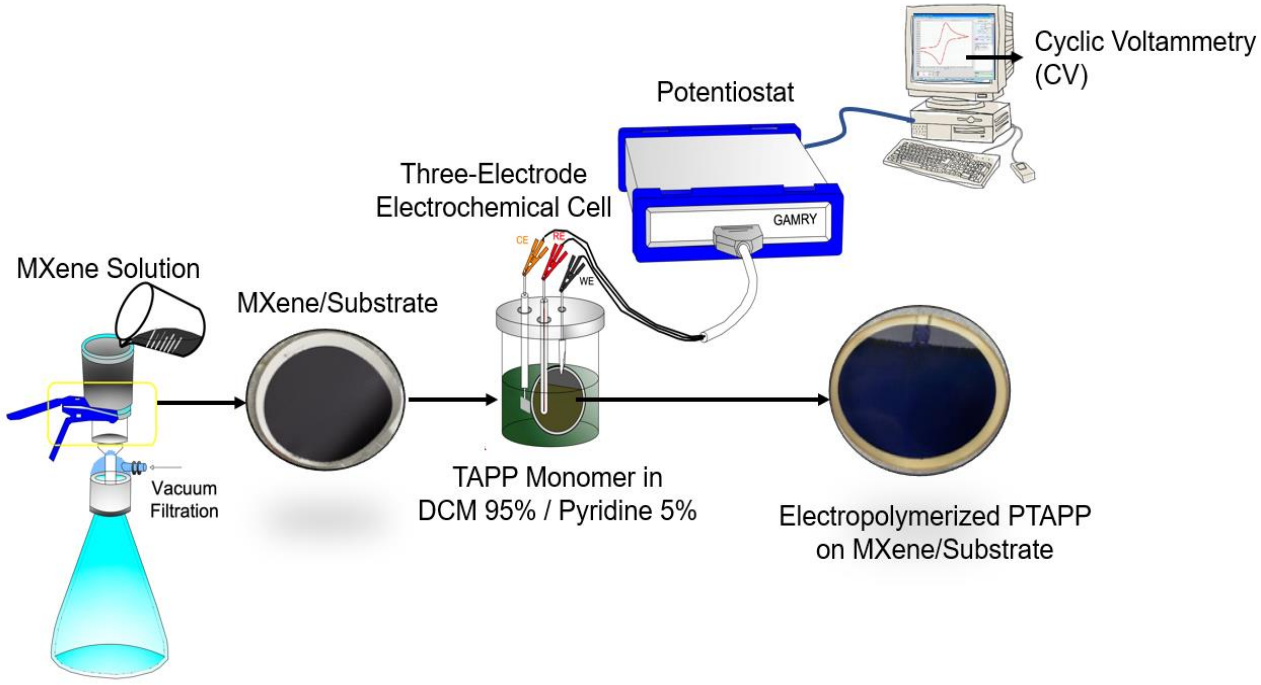

Figure 3.7 *The schematic of PTAPP/MXene Membrane Fabrication*

3.4.2.1 Pre-deposited Membrane Fabrication

In the pursuit of well-defined film pores, herein, for the first time, the use of MXene is considerable as conductive material instead of using ITO glass. As shown in **Figure 3.7**, MXene is deposited on porous substrates, via vacuum filtration with various mass loading to represent the thickness and the conductance of the MXene membrane. The optimal deposition of MXene on substrate determines the high oxidative polymerization of TAPP monomer during the electropolymerization process, in which a densely formed thin layer is obtained. Here, the deposition of MXene 3 - 8 mg was chosen for experiment.

3.4.2.2 Electropolymerization of PTAPP film on MXene/Substrate Membrane

The overall mechanism of electropolymerization is similar to that of PTAPP film on ITO glass; however, in this part, the solid working electrode is the MXene surface layer, which is previously deposited on the substrate. TAPP solution contained 0.5 mM of TAPP monomer concentration, 0.05 M TBAPF6, and 5% v/v pyridine solution. MXene/Substrate membrane in TAPP solution was vertically kept sitting upright to obtain sufficient surface area for deposition of PTAPP. Processing parameters, except scan rates and monomer concentration, were fixed. Since the oxidized TAPP monomer is directly deposited MXene/Substrate membrane, the free-standing film is no longer necessary, and the membrane is ready for use. As-prepared membranes were washed using acetonitrile (CH_3CN) to remove unreacted monomers and the remaining supporting electrolyte.

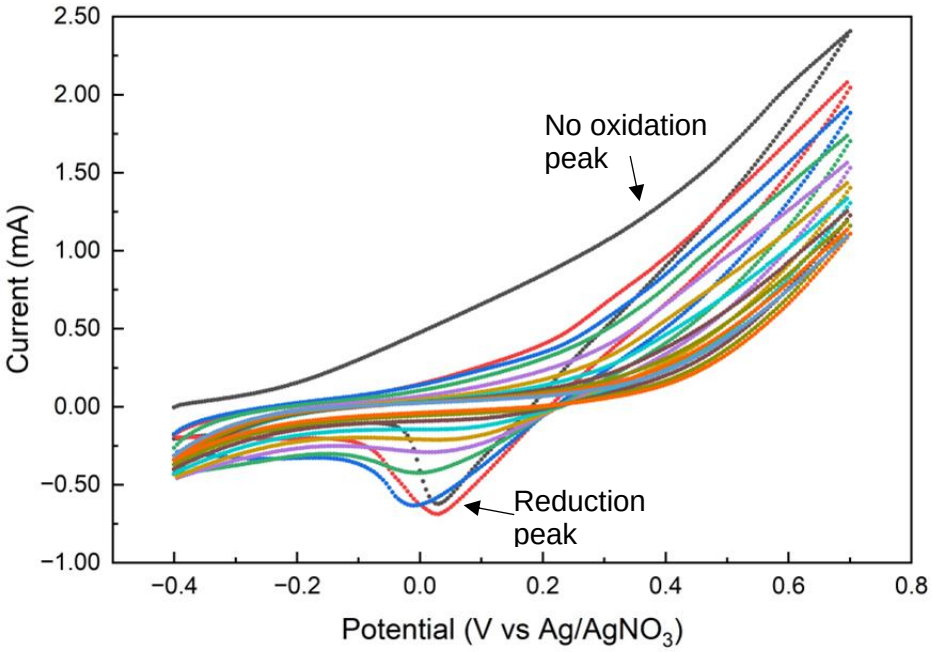

Figure 3.8 *The cyclic voltammogram of TAPP electropolymerization on MXene/Substrate using a scan rate of 10 mV/s at room temperature, performed in 0.5 mM TAPP, 0.05 M TBAPF6, and 5 % v/v pyridine solution*

3.5 Membrane Testing Performance

The separation performance of membrane was assessed in two different operational systems: pressure-driven process in dead end-cell and osmotically driven in static diffusion cell.

3.5.1 Dead End Cell

The prepared membranes were further tested in a pressure-driven separation process. The dead-end filtration set-up is shown in **Figure 3.9**. The pressure of 100 psi was applied for two-layer PTAPP membrane, while the pressure of 10 - 35 psi was applied for three-layer PTAPP membrane. A 10-ppm Reactive-Black-5 (RB-5) dye solution in methanol was used for all experimental codes of membrane tested. The membrane area was adjusted to 0.000078 m^2. The permeate solution was collected in 30 minutes and the weight was monitored by digital balance.

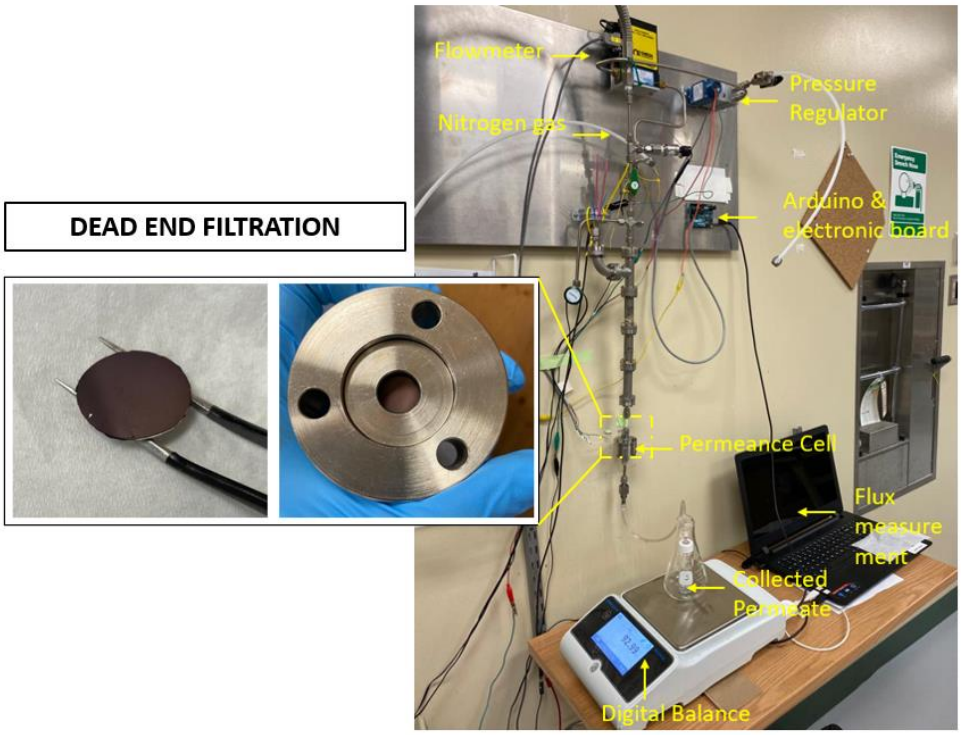

Figure 3.9 (a) and (b) preparation of membrane into permeance Cell, and (c) dead-end filtration set-up

Each measurement was repeated three times to obtain the average values of permeance and rejection, which were calculated through the following equations:

$$J = \frac{V}{A \times \Delta t} \quad \text{(Equation 3.1)}$$

$$\text{Permeance} = \frac{J}{P} \quad \text{(Equation 3.2)}$$

$$R = \frac{C_f - C_p}{C_f} \times 100\% \quad \text{(Equation 3.3)}$$

where J is a flux (L m^{-2} h^{-1}), V is the volume of permeate solution (L) collected over a period of time Δt (h), A is the effective surface area in the unit of m^{-2}, P is the applied pressure, R is the dye rejection (%), C_f is the concentration of feed solution, and C_p is the concentration of permeate solution collected. The dye rejection in feed and permeate solution was measured using UV-Vis Spectroscopy.

3.5.2 Static Diffusion Cell

The principle of static diffusion cell, like the diaphragm-cell diffusion discussed by Cassler (2009) involves two well-stirred volumes separated by a thin-porous barrier, as shown in **Figure 3.10**. The concentration of upper and lower compartments was measured after a known time and diffusion coefficient can be calculated.

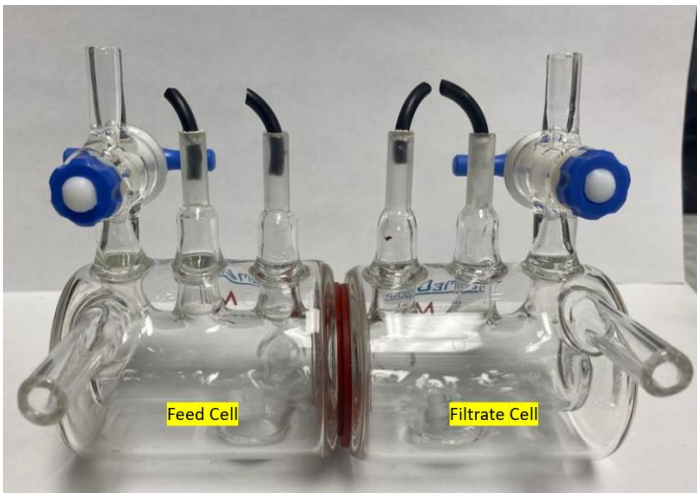

Figure 3.10 *Static Diffusion Cell*

The separation performance of Sodium Chloride (NaCl) was performed using static diffusion cell. In this work, the feed chamber was filled by NaCl, 0.1 M solution and the filtrate chamber was filled by deionized (DI) water. Electrodeposited PTAPP film was prepared using 0.5 mM TAPP concentration, 10 mV/s scan rates, and 10 cycles. Then, free-standing film was transferred on Nylon, and the bottom PTAPP film was used as the upper layer of the PTAPP membrane. Besides the rejection, diffusion phenomenon was also observed in salt separation.

The diffusion rate is commonly interpreted in Fick's diffusion law. In Fick's law, unit time per through unit area per diffusive flux of materials is proportional to the concentration gradient.

$$J_A \propto \frac{dc_A}{dz} \; or \; J_A = -D_{AB} \frac{dc_A}{dz} \qquad \text{(Equation 3.4)}$$

J_A is the mole diffusive flux, $kmol.m^{-2}s^{-1}$, z is distance of diffusion direction, $\frac{dc_A}{dz}$ is concentration gradient of component A at z-direction, $kmol/m^3$, and D_{AB} is diffusion coefficient of component A in component B.

In the pseudo-steady state, the flux across the thin-porous barrier is that given for membrane diffusion.

$$j_1 = \left[\frac{DH}{l}\right]\left(C_{1,lower} - C_{2,upper}\right) \qquad \text{(Equation 3.5)}$$

Here, the quantity H includes the fraction of the diaphragm's area that is available for diffusion. The overall mass balance on the adjacent compartments as follow:

$$V_{lower} \frac{dC_{1,lower}}{dt} = -Aj_1 \; , \; V_{upper} \frac{dC_{2,,upper}}{dt} = +Aj_1 \qquad \text{(Equation 3.6)}$$

A is the diaphragm's area. If these mass balances are divided by V_{lower} and V_{upper}, respectively, and the equations are subtracted, one can combine the result with the flux equation to obtain

$$\frac{d}{dt}\left(C_{1,lower} - C_{2,upper}\right) = D\beta\left(C_{2,upper} - C_{1,lower}\right) \quad \text{(Equation 3.7)}$$

in which

$$\beta = \frac{AH}{l}\left(\frac{1}{V_{lower}} + \frac{1}{V_{upper}}\right) \quad \text{(Equation 3.8)}$$

is a geometrical constant characteristic of the diaphragm cell being used. This differential equation is subject to the obvious initial condition

$$t = 0, \quad C_{1,lower} - C_{2,upper} = C^0_{1,lower} - C^0_{2,upper}$$

If the upper compartment is initially filled with solvent, then its initial solute concentration will be zero. Integrating the differential equation subject to this condition gives the desired result:

$$D = \frac{1}{\beta t}\left(\frac{C^0_{1,lower} - C^0_{2,upper}}{C_{1,lower} - C_{2,upper}}\right) \quad \text{(Equation 3.9)}$$

In other work, using static diffusion cell, the sized-based selectivity was performed. Electrodeposited PTAPP film was prepared using 0.5 mM TAPP concentration, 10 mV/s scan rates, and 10 cycles. Then, free-standing film was transferred on Polyethylene (PE), and the top PTAPP film was used as the upper layer of the PTAPP membrane. The feed solution was the mixtures of two different dyes in methanol, 50 ppm with ratio 1:1. The first mixture was Congo Red (CR, Mw = 696.665) and Methyl Blue (MB, Mw = 799.814), and the second mixture was Congo Red (CR, Mw = 696.665) and Methyl Orange (MO, Mw = 327.33). The filtrate chamber was filled with pure methanol. During the experiment, the stirring was on in both chambers to prevent the concentration polarization.

3.6 Characterization

The asymmetry and surface structure of prepared membranes were examined with scanning electron microscopy (SEM) (NanoSEM450 and FEI Helios) in Nebraska Center for Materials and Nanoscience (NCMN), University of Nebraska-Lincoln. The chemistry of electrodeposited PTAPP on substrate or MXene/substrate membrane was evaluated using Fourier-Transform Infrared Spectroscopy (FT-IR) in Transformative Coating and Interface Laboratory (TCIL), University of Nebraska-Lincoln.

CHAPTER FOUR: RESULT AND DISCUSSION

4.1 Bilayer PTAPP Membrane

4.1.1 Electropolymerization of PTAPP film on ITO Substrate

The electropolymerization mechanism of PTAPP film is chemically irreversible reactions that are monitored by cyclic voltammetry (CV). The reaction process undergoes oxidation first, in which the potential is scanned from low potential to high potential; then followed by reduction upon scanning back to low potential.

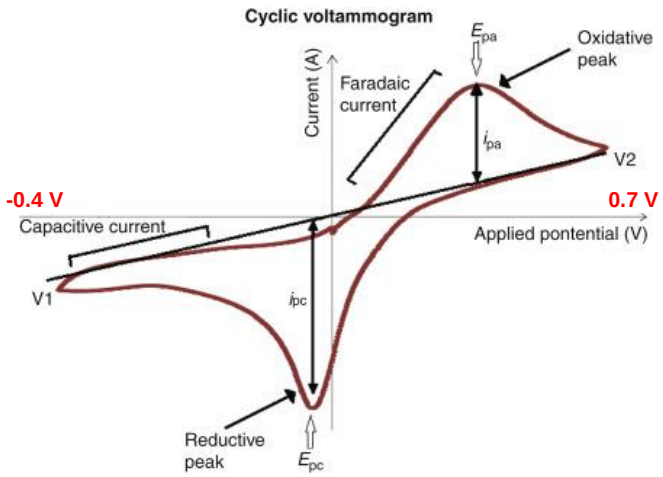

Figure 4.1 *Schematic diagram of a cyclic voltammagram highlighting the peak cathodic potential (Epc), peak anodic potential (Epa), oxidation peak and reduction peak.*

In the experimental work, oxidation occurs when the potential is scanned positively from -0.4 V to 0.7 V (anodic region). While TAPP monomer in DCM solvent is electrochemically oxidized at the surface of the electrode, transferred electrons are occurring from molecule to the electrode because of potential energy; therefore, PTAPP film slowly deposits on the surface. After reaching the switching potential at 0.7 V, the scanning potential is switched in the opposite direction, from 0.7 V to -0.4 V (cathodic region); here, the reduction occurs. Peaks in the anodic and cathodic regions indicate the complete redox reactions, which means all the active monomers at the surface have been oxidized and reduced. Irreversible transfer electrons are indicated by individual peaks which separate in the wide distance.

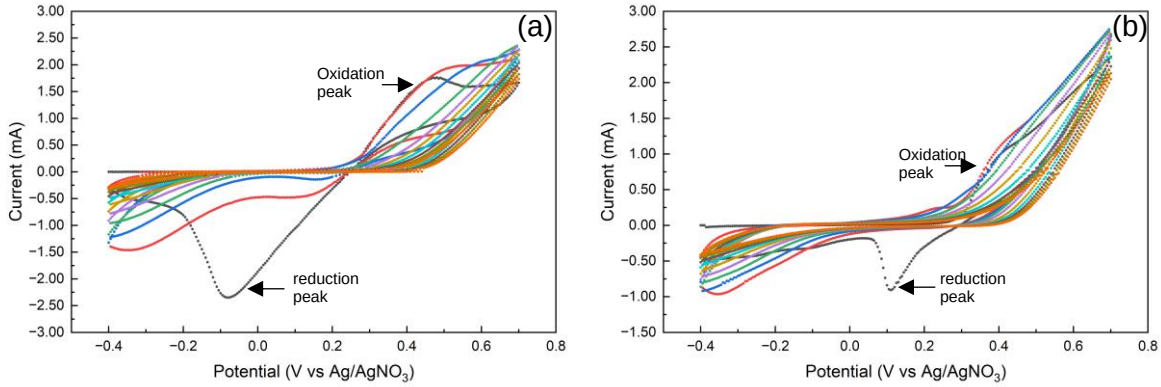

Figure 4.2 *Cyclic voltammogram of (a) electropolymerized PTAPP film, and (b) electropolymerized PTAPP/Cu-TAPP film, using a scan rate of 10 mV/s, performed in 1.0 mM TAPP or mixed TAPP/Cu-TAPP monomer in DCM, 0.05 M TBAPF6, and 5% v/v pyridine solution*

In this study, electropolymerized PTAPP films with different processing parameters were observed based on a cyclic voltammogram (CV) curve. In monomer type experiment, this study attempted to compare two electropolymerized films that contain a single TAPP and mixed TAPP and Cu-TAPP monomer, respectively. As shown in **Figure 4.2**, CV curves of both electropolymerizations have different shapes. The electropolymerization of PTAPP film, with TAPP monomer only (**Figure 4.2(a)**), revealed the visible oxidation and reduction peaks; in contrast, the electropolymerization of film with the mixed monomer (**Figure 4.2(b)**), peaks are reduced in size, and the peak that represents oxidation is not clearly visible.

The significant difference was found in the direction of diffusion behavior. In principle, during the electropolymerization process, the mass transport of analytes that approach the electrode surface is favored by diffusion. However, as the portion of active monomers is depleted at electrode surface, the concentration decreases. Less concentration causes the random motion of monomers, and diffusion is limited by the distance of monomers from the surface. Hence, smaller active monomers can be diffused to the electrode. This phenomenon explains the decreasing currents after the oxidation peak is reached, as shown in **Figure 4.1(a)**. Reversibly, currents appeared to increase after hitting the oxidation peak, as shown in

Figure 4.2(b), indicating that large amount of active monomers at the electrode surface after oxidation process, and diffusion layer is thin.

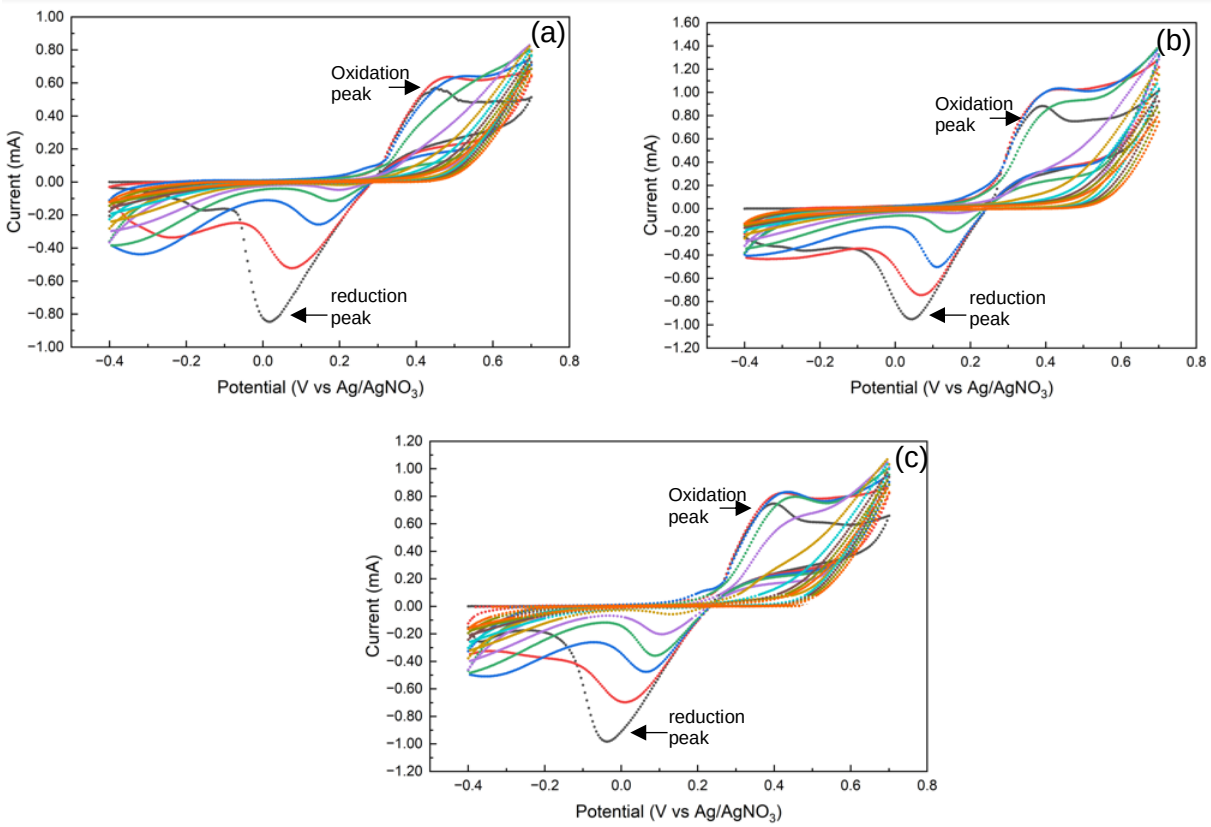

Figure 4.3 *The Cyclic Voltammogram of Electropolymerized PTAPP film using various a scan rate, (a) 5 mV/s, (b) 10 mV/s, and (c) 15 mV/s, performed in 0.5 mM TAPP monomer in DCM, 0.05 M TBAPF6, and 5% v/v pyridine solution*

The resulting current is dependent on the scan rate applied and is inversely proportional to diffusion layer thickness. Higher currents are achieved as the scan rate is rapid and the size of the diffusion layer is reduced (Elgishri, 2018). As shown in **Figure 4.3**, the electropolymerization using 10 mV/s resulted in a higher current compared to that using 5 mV/s. It was assumed that the oxidized monomer at the electrode surface forms a barrier called a diffusion layer. At slower scan rates, 5 mV/s, the diffusion layer is thick due to the mass oxidized monomer at the electrode surface. Consequently, the mass transport of monomers via diffusion slowly declines, leading to slower and slower the resulting current.

However, contrary to the theoretical view, the electropolymerization using 15 mV/s is not as expected as the resulting currents are almost identical to that using 10 mV/s.

To further the finding, sluggish charge transfers kinetic (Elgrishi et al., 2018) and a single wave with no return peak in the bottom are typical irreversible reactions. Return peak refers to reduction peak, and it is considered not to occur because the product is permanently formed at the surface of the electrode. However, at higher concentrations (**Figure 4.2**), the reduction peak was found only in the first cycle. By contrast, at 0.5 mM concentration (**Figure 4.3**), the varying reduction peaks were observed in any cycles for all electropolymerization using different scan rates. Moreover, the observed reduction peak is usually considered as another half of redox reactions. However, in the experimental works, the peak currents in cathodic regions are mostly higher than those in anodic regions. This indicates that the product (oxidized TAPP) may be simultaneously reduced to the actual monomer and other forms.

4.1.2 Scalability

Several fabrication methods, such as interfacial polymerization and initiated or oxidative chemical vapor deposition (iCVD or oCVD) have shown promise in fabricating scalable polymer membranes with tunable properties. However, the inert material of film plagues the practices when the production is sized up, leading to defects, heterogeneous pores, and functional deficiencies in performance. Nevertheless, discussion on advanced methods for large-produced film is still a trending topic, and one appealing technology recently taking part in this interest is electropolymerization. Interestingly, processing parameters in electropolymerization are scalable; therefore, control over the thickness is gained. Moreover, thin-film size can be enlarged without additional chemicals and processing but still offers tailored properties.

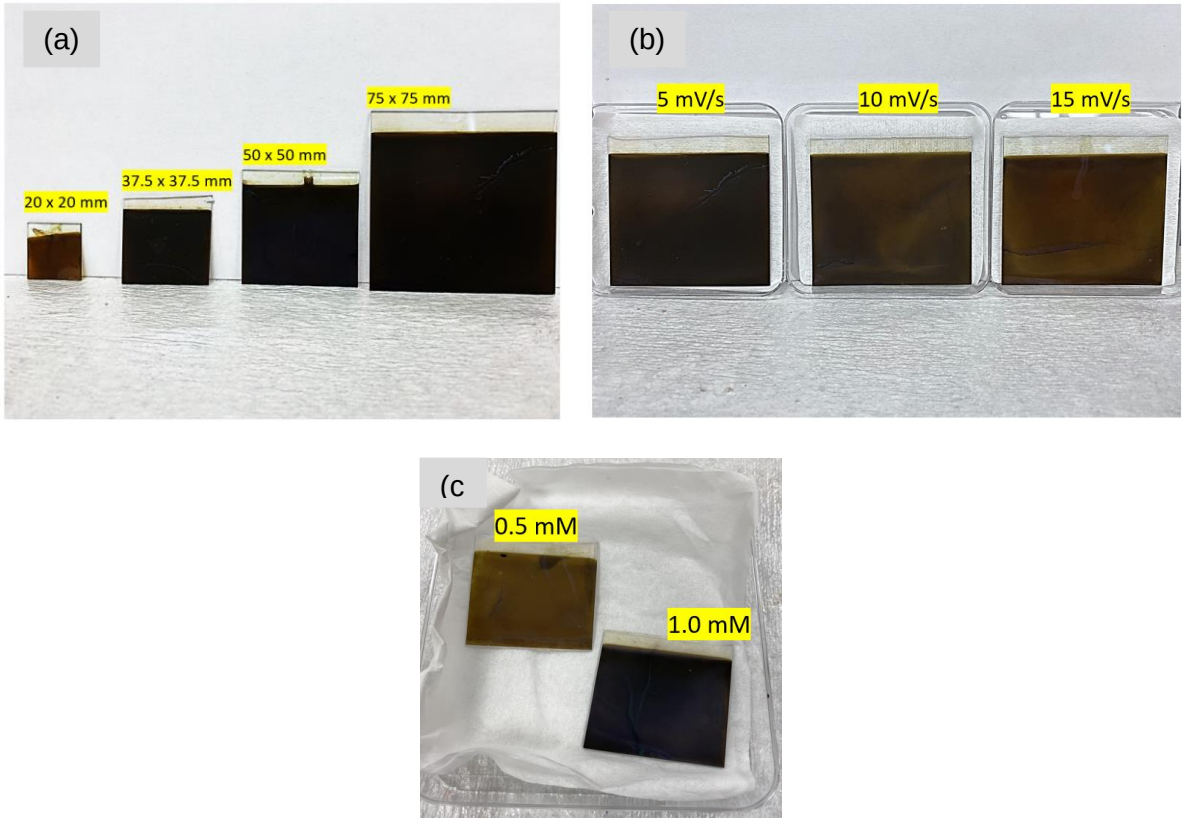

Figure 4.4 *Demonstration of scalability of (a) surface area based on ITO glass size and (b) and (c) thickness based on scan rate and concentration, performed in 0.5 – 1.0 mM TAPP in DCM monomer, 0.05 M TBAPF6, and 5% v/v pyridine solution*

This study demonstrated the successful scalability of the electropolymerized PTAPP film in terms of surface area and thickness. As shown in **Figure 4.4(a)**, PTAPP film can be electropolymerized on various sizes of ITO glass, starting from 20 mm to 75 mm in dimensional length. No defects were observed on the film surface, indicating uniform density. Another scalable parameter is the scan rate, up to 15 mV/s, which produces different film thicknesses. In **Figure 4.4(b)**, the darker brown-color film by 5 mv/s represents the mass deposition of PTAPP on ITO glass. Besides scan rates, the thickness can be controlled by adjusting the concentration of TAPP monomer in the solution. As discussed in the previous section, the higher concentration makes the TAPP monomer more accessible to the electrode surface via diffusion, and this system favors the forming film, indicated by the darker color at a concentration of 1.0 mM shown in **Figure 4.4(c)**. This result is in agreement with

Kellenberger (2014) and El Aggadi et al. (2020) that the greater mass loading on the surface of electrode correlates with the higher concentration of active monomer in the double layer and increased oxidative polymerization at low potential scan rate. Therefore, the conveniences in scalability lead this electrochemically formed film to potential in the industrial sector.

4.1.3 State-of-art free standing film

Free-standing film is an effective method for releasing film from its substrate, an ITO glass. KOH plays an important role in the delamination process. The effect of using concentrated KOH is to create a gap between the PTAPP layer and substrate, by etching indium thin oxide and removes impurities such as unreacted TAPP monomers. It is important to note that the use of low concentrated KOH has the potential to cause defects and fractions because KOH is not able to etch ITO glass surfaces; therefore, efficient concentration is very necessary. Free-standing film with various concentrations of KOH, and it was found that well-delaminated film was obtained using 8 M KOH. In this demonstration, the surface of PTAPP film (on ITO glass substrate) is scratched on edge sides, it is then immersed in DI water, and added 8 M KOH slowly dropwise.

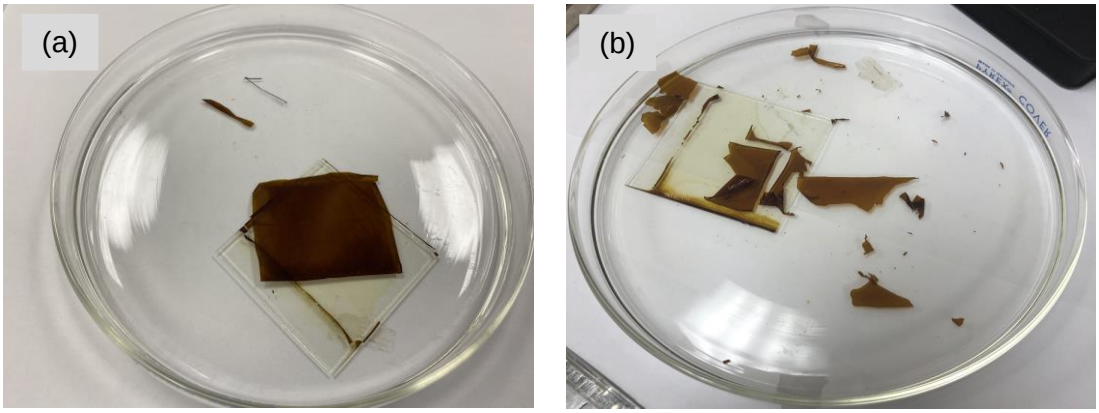

Figure 4.5 *The Digital photographic images of free Standing PTAPP film (a) well-delaminated film, and b) poorly delaminated Film, performed in 0.5 – 1.0 mM TAPP monomer in DCM, 0.05 M TBAPF6, and 5% v/v pyridine solution*

Free-standing PTAPP films were nicely obtained using chemical etching by KOH. As observed, the amount of concentrated KOH added to DI water, in which the PTAPP film on ITO is immersed, varies depending on the physiochemical properties of the electropolymerized PTAPP film. The droplets of 8 M KOH using a 3-ml plastic pipet were added two times in the beginning, and delamination occurred in 30 - 90 minutes. However, in some cases, delamination takes longer, and the concentrated KOH is increasingly added. A successful free-standing film can be obtained if the PTAPP film is electropolymerized in normal systems where there are no impurities in the solution. The impurities, for example TBAPF6 without further purification process, interferes the stability of electropolymerized PTAPP film. On trials, mechanically unstable film due to impure TBAPF6 is more vulnerable to break during lift-off process, as shown in **Figure 4.5(b)**. Other crucial considerations are the cleanliness of electrodes and ITO glass substrate; they should be free from any organic substances.

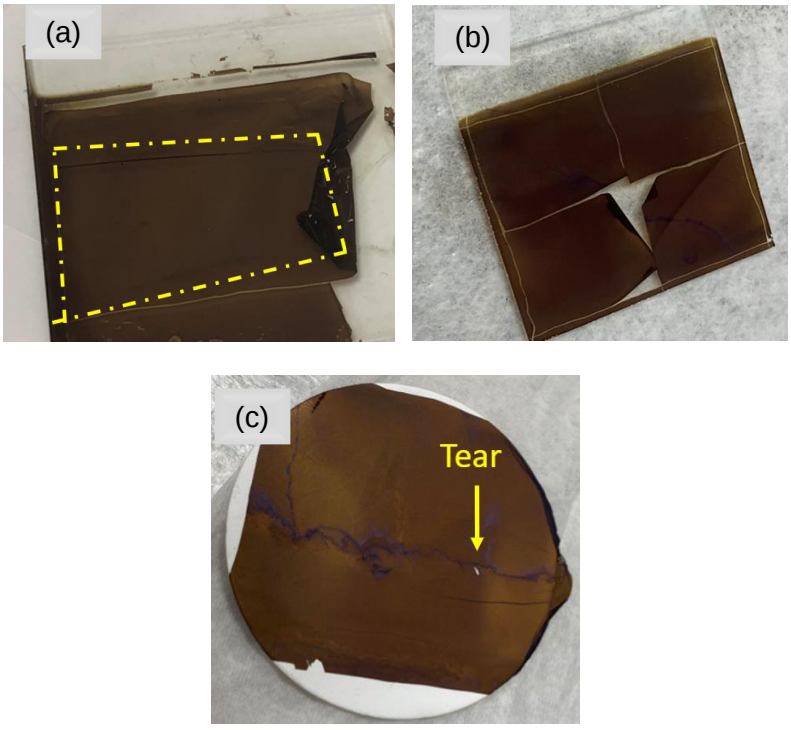

Figure 4.6 *Digital photographic Image of delamination process after KOH concentration is added (a) large area film, b) adjusted area film, c) tear on film after transferred, performed in 0.5 – 1.0 mM TAPP monomer in DCM, 0.05 M TBAPF6, and 5% v/v pyridine solution*

The delamination process usually starts from the edge, close to the etched area, because that place is where the concentrated KOH first enters between the PTAPP film and the ITO glass substrate. However, delamination faces obstacles if the film has a large area. When the delamination reaches the center area of the film, at this point, there is some portion of the film area underneath that needs extra time to delaminate as shown in **Figure 4.6(a)**. As a result, the film is prone to forming tears in the center area, shown in **Figure 4.6(c)**. In theoretical view, the interfacial peeling energy and the swelling-induced strain energy determines the minimum film thickness that can be released (Suresh and Freund, 2003). The safest approach is to add KOH and give extra time for the film to lift off. Another solution is that if the intended membrane is small, the area of the film can be adjusted by etching the center area of the film, as shown in **Figure 4.6(b).**

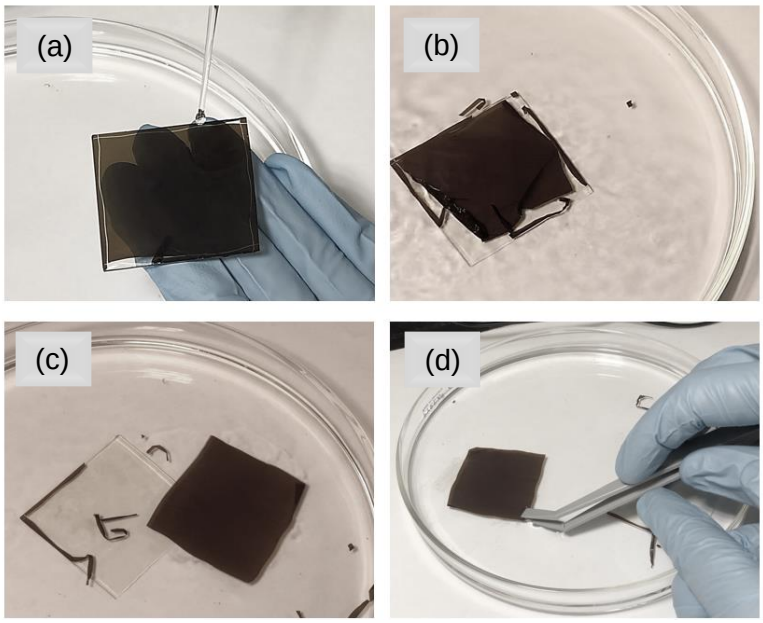

Figure 4.7 *Digital photographic images of free standing PTAPP film using ethanol, (a) the dropping ethanol on top film surface, (b) the delamination process, (c) and (d) free-standing film, performed in 0.5 – 1.0 mM TAPP monomer in DCM, 0.05 M TBAPF6, and 5% v/v pyridine*

To the best knowledge of the state-of-art free-standing porphyrin film, this study investigated the delamination facilitated by ethanol (**Figure 4.7**). Films that have a high thickness have mechanical stability. The electropolymerized film using 5 mV/s, for instance, has dense film underneath, which is strongly binding with the ITO substrate; thus, it is difficult to make a gap between layers, no matter how much KOH has been added. This study attempted to improvise by adding ethanol on top surface film thoroughly, leaving it for 15 seconds, and then putting it back into KOH/H_2O solution. While the KOH facilitates the etching of indium tin oxide underneath the PTAPP film, the top film surface is gently delaminated due to the surface tension in response to the addition of ethanol. Surprisingly, in less than 5 seconds, the film lifts off spontaneously without any damage.

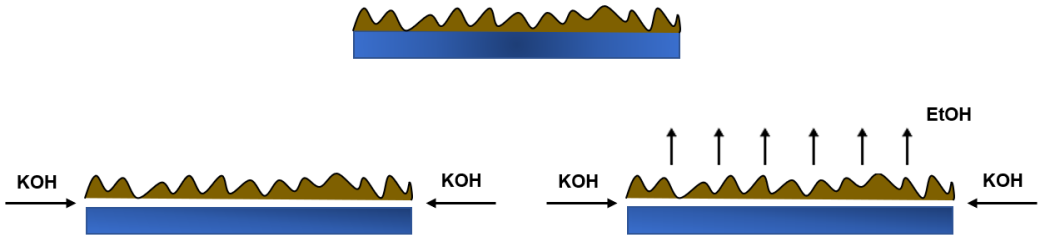

Figure 4.8 *The illustration of free-standing PTAPP film using KOH in H_2O solution only and KOH in H_2O solution and ethanol*

During delamination process, the KOH etches the indium tin oxide from PTAPP underneath, the ethanol attracts PTAPP from top simultaneously as illustrated in **Figure 8**. The droplets of ethanol added on top film surface do not mix water immediately, however they have strong adhesion with solid organic material, PTAPP film.

4.1.4 SEM Characterization

The morphology and structure of deposited PTAPP film were performed using scanning electron microscopy (SEM). The prepared samples are electropolymerized PTAPP films with various monomer types and scan rates. Simultaneously, this study discussed the top and bottom surfaces of PTAPP film. The surface morphology of PTAPP films displays wire-like porous structure, characterized by nanofibrous with thickness range of 25 to 75 nm and pore size of 10 to 50 nm (Walter and Wamser, 2010).

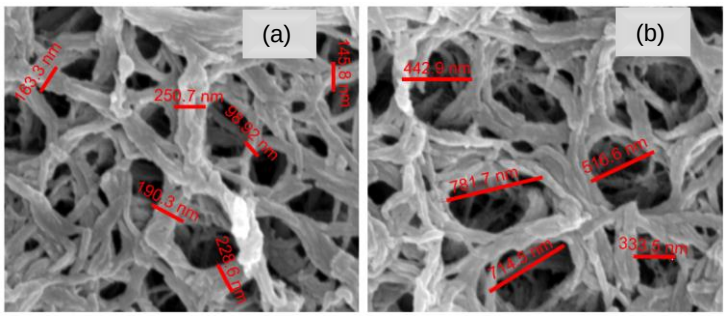

Figure 4.9 *SEM images of PTAPP film morphology includes (a) nanofiber length and (b) pore size, using scan rate of 10 mV/s through 10 cycles, performed in 1.0 mM TAPP monomer in DCM, 0.05 M TBAPF6, and 5% v/v pyridine*

In the original version, the PTAPP structure (**Figure 4.9**) is typically signature by the wire-like or finger-like, with thickness more than > 100 nm and pore size range of 300 – 800 nm. Interconnections between fibrous form nanopores liable for channeling molecules based on size level. Another advantage of this crystalizing network is the high surface area, which means more sites for binding ions during the separation process.

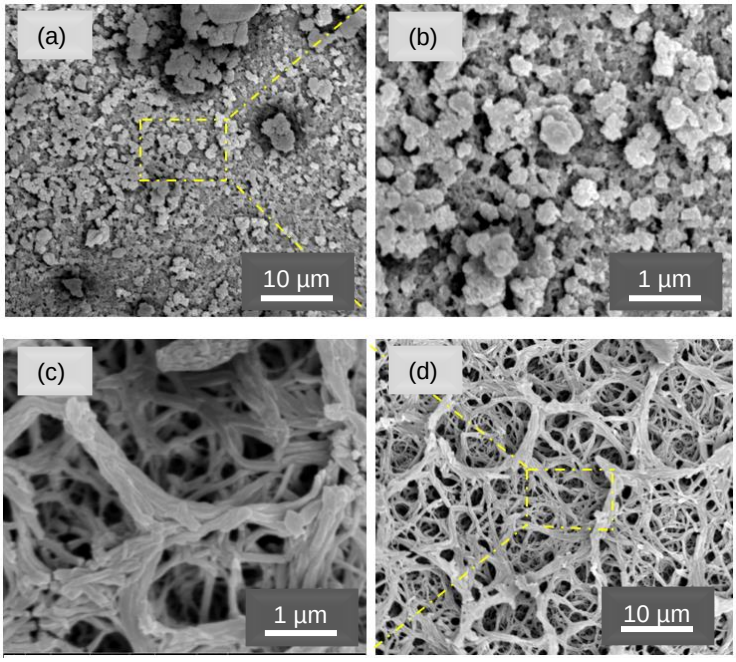

Figure 4.10 *SEM images of (a) and (b) PTAPP/Cu-PTAPP film and (c) and (d) PTAPP film morphology using scan rate of 10 mV/s through 10 cycles, performed in 1.0 mM TAPP monomer in DCM, 0.05 M TBAPF6, and 5% v/v pyridine*

To extent the understanding of PTAPP morphology in respect to various processing parameters, this study explored the significant difference in surface morphology between electropolymerized PTAPP single only and electropolymerized PTAPP containing Cupper (Cu) metal ions in monomers. As shown in **Figure 4.10**, the surface of PTAPP/Cu-PTAPP film possesses robust crystallinity and uniform density with pore size at the nanoscale, compared to the original version (PTAPP film without metal ions). The presence of Cupper metal ions in the monomer as a functional group endows a denser and rougher film surface, and the structure portrayed is more stone-like.

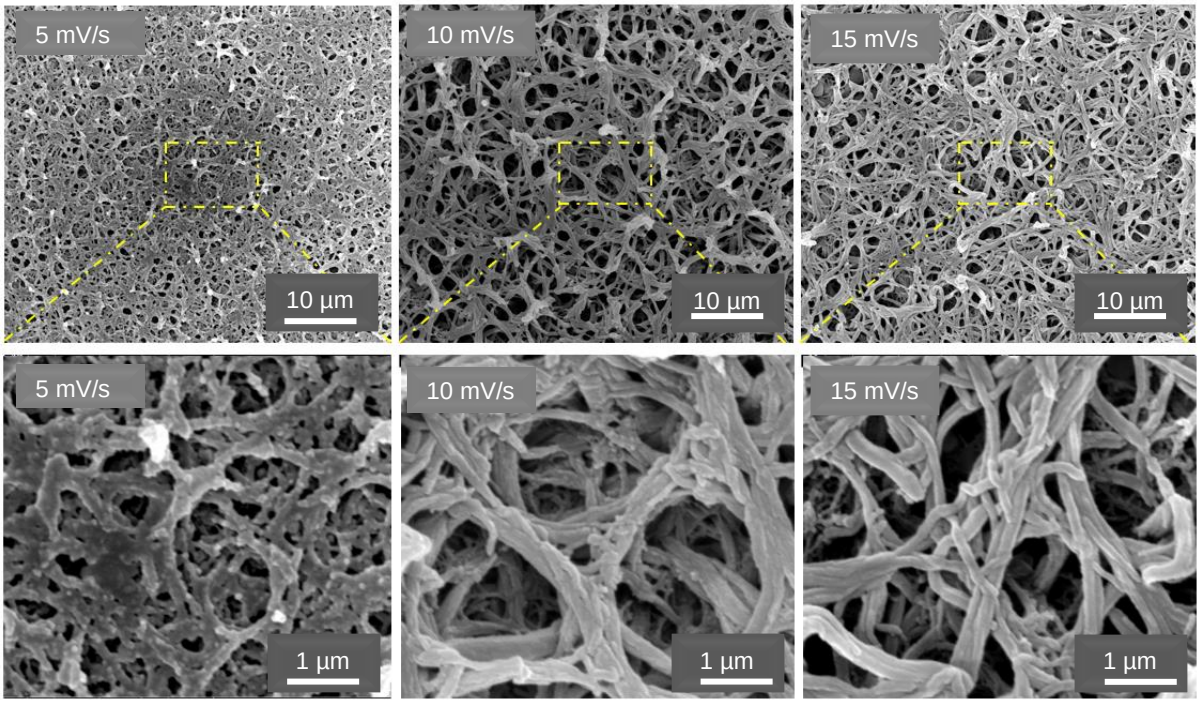

Figure 4.11 *SEM images of PTAPP film morphology using various scan rates through 10 cycles, performed in 1.0 mM TAPP monomer in DCM, 0.05 M TBAPF6, and 5% v/v pyridine*

Electrodeposited PTAPP film with different potential scan rates were displayed in **Figure 4.11**. In line with expectations, the structure and uniformity are different among them. The nanofiber diameter of PTAPP film using 5 mV/s is wider and showed the highly-cross-linked structure. As the scan rate increases, the nanofiber diameter dwindles, further indicating a decrease in oxidative polymerization. In the observation, smaller finger-like structures advantage a greater

surface area; however, the mechanical strength of interconnected nanofibers may not as bond as those structures with lower scan rates (5 - 10 mV/s), and potentially impact on delamination process in the free-standing film. In some cases, the structure of PTPP film electropolymerized with 10 mV/s and 15 mV/s are not significantly different. The continued oxidative polymerization such as coupling reactions may occur on the electrode; at this point, the poly-TAPP layer is still forming, even the complete oxidation is achieved, on cyclic voltammogram (CV).

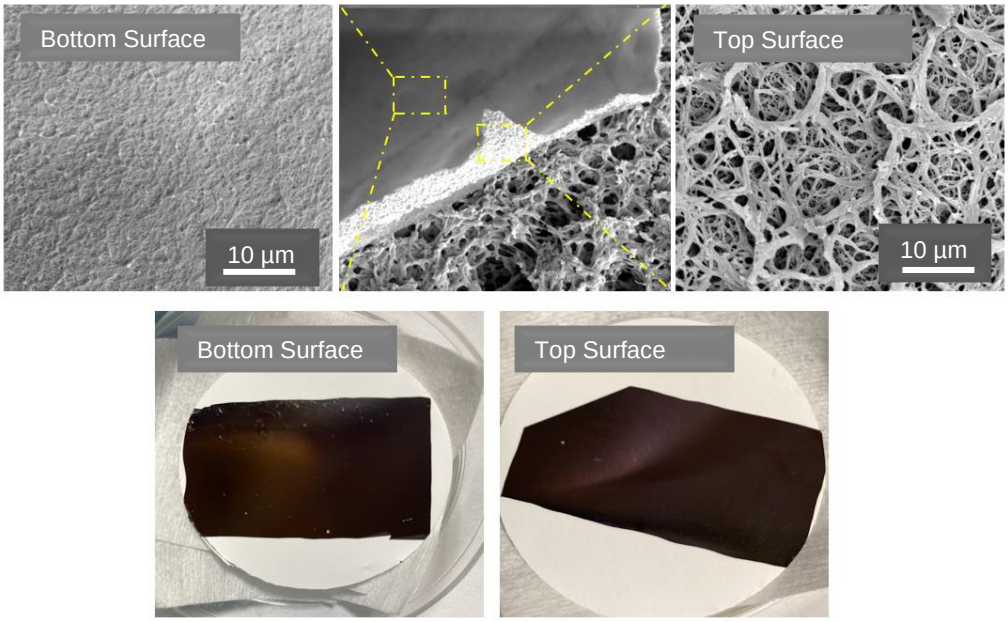

Figure 4.12 *SEM and digital photographic images of top and bottom PTAPP film morphology using scan rate 10 mV/s through 10 cycles, performed in 0.5 - 1.0 mM TAPP monomer in DCM, 0.05 M TBAPF6, and 5% v/v pyridine*

The next exploration is the surface morphology of top and bottom PTAPP film. As shown in **Figure 4.12**, the top and bottom surface of PTAPP film has different visualizations associated with density, which the bottom one is densely-form PTAPP. It is important to note that the ITO substrate has a dense and smooth conductive area, and the growth of PTAPP film follows the substrate morphology. Active monomers with the closest contact with the electrode surface are readily oxidized on the surface. PTAPP is electronically conductive, and the linked monomers units by bridging groups offer electron conductivity. When the area of conductive

substrate is fully grown by the PTAPP film, in this case, the formed film starts making a fracture on the top region by coupling reactions to form the polymer.

The described process above is in line with the conceptual mechanism of electropolymerization. Polymerization is carried out by the coupling between radical cations or the reaction of radical cations with a neutral monomer. Radical cations are species originated from the oxidation of monomer at given potential; in this study, radical cations refer to the formed PTAPP film on the electrode surface, afterwards they couple with the TAPP monomer. In other words, the top surface film is formed from fractionization or continued crystallization from the bottom. Therefore, the bottom surface of PTAPP film displays a denser morphology whereas the top surface morphology is more porous. Additionally, by observing the digital photos of transferred PTAPP films (top and bottom) on support (**Figure 4.12**), the bottom film surface as the upper looks shiny and darker brown, compared to the top film surface. The rough calculation of pore size benzene ring linkages is 1.32 nm **(Appendix B)**. These observations indicated that this film, especially the bottom region has sub nanopores, which are approximately 1 nm.

4.1.5 Dead End Filtration

The as-prepared membranes with various processing parameters were tested using dead-end cells to evaluate the permeance and rejection against the organic solvent. Surprisingly, the variability was observed for each membrane in three-time measurements. In the case of scan rates, PTAPP/Nylon membranes with a 15-mV/s electropolymerized film are the most variable, indicated by the error bar. This significant deviance is influenced by the nature of the finger-like structure and the nanofibrous network, as discussed in **sub-section 4.1.4**. The weak mechanical strength characterized by thinner nanofibers is susceptible to defection and cracking during the experiment. Moreover, the film was in direct contact with the solvent, putting the film under harsh conditions. During compaction, the solvent permeated through the pores. Simultaneously, it deteriorated the constructed network of PTAPP film, then finally

contributed to the defect. Therefore, in this work, the 15 mV/s PTAPP/Nylon Membrane is not an ideal design

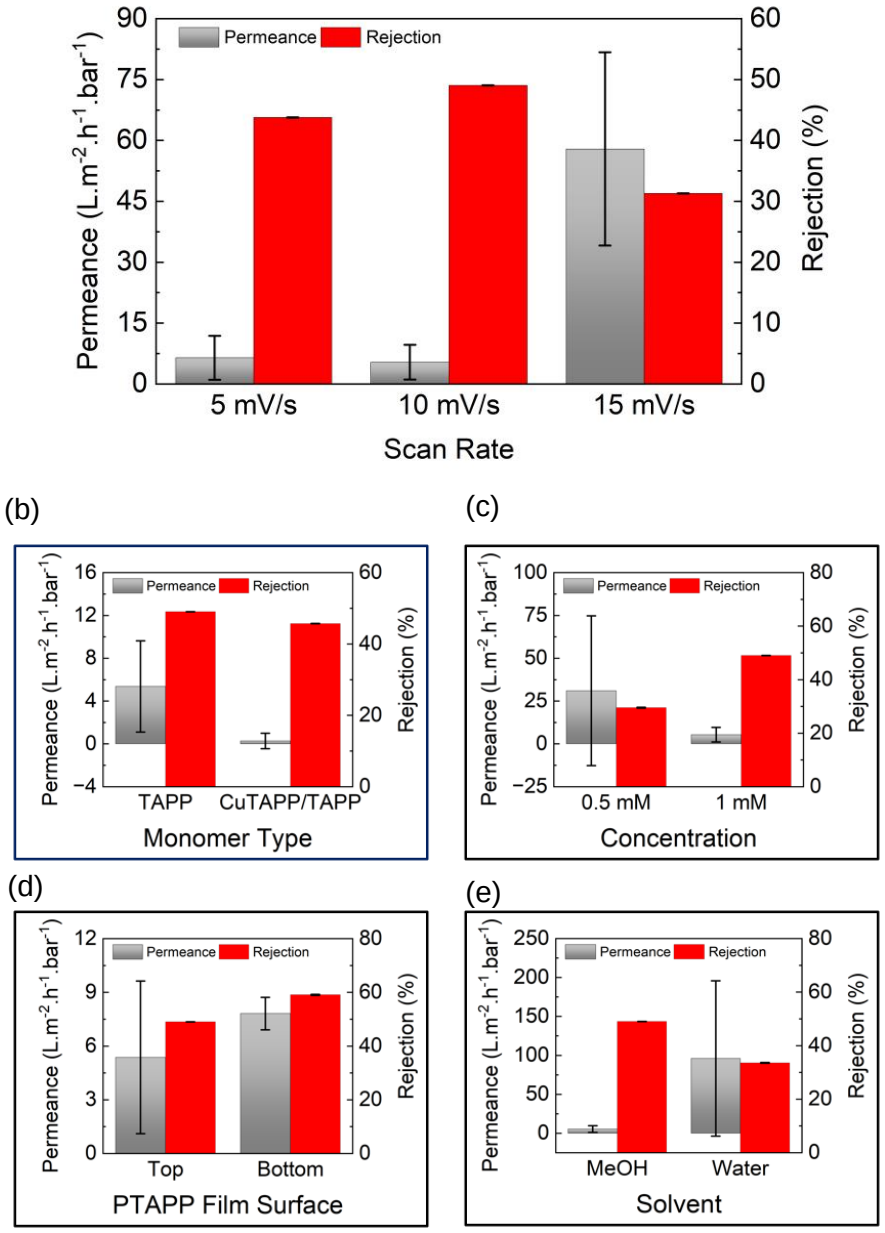

Figure 4.13 *Separation performance of PTAPP/Nylon membrane, using electropolymerized PTAPP Film with various processing parameters, toward Reactive Black -5 (RB-5) dye in methanol.*

Regarding hierarchical thickness based on scan rates, the permeance performance unpredictably breaks the order. As shown in **Figure 4.13(a)**, the order of permeance was

6.46 $L.m^{-2}.h^{-1}.bar^{-1}$, 5.37 $L.m^{-2}.h^{-1}.bar^{-1}$, and 57.90 $L.m^{-2}.h^{-1}.bar^{-1}$, performed by 15 mV/s, 5 mV/s, and 10 mV/s PTAPP membranes, respectively. A 15 mV/s PTAPP membrane exhibited the highest permeance because of its vulnerability to organic solvents and weakly-interconnected structure.

In **sub-section 4.1.4**, the electropolymerized PTAPP film, with a scan rate of 5 mV/s, portrayed the rigid and robust structure and the massive deposition as a function of thickness. However, in this experimental work, this film did not show a satisfying performance as expected. The permeance of 5 mV/s PTAPP membrane was relatively low but slightly higher than that of the 10 mV/s PTAPP membrane. This narrow permeance verified the remaining unreacted TAPP monomers and PTAPP oligomers in the pore films; hence limiting the active surface area and the transport. In addition, when the membrane is under applied pressure, the compaction physically triggers the deformation of pore geometry. The compaction of membrane restricts the solvent transport; hence, less permeate is obtained.

The rejection values for each membrane were achieved with minor errors. The rejection values, like permeance did not show a clear relationship with scan rate, but their values corresponded to the permeance. A 10 mV/s PTAPP membrane revealed about 49.05% rejection toward dye, while a 5 mV/s and 15 mV/s PTAPP membrane showed 43.78% and 31.30 % rejection, respectively. PTAPP/Cu-PTAPP membrane (**Figure 4.13(b)**) performed a similar rejection value, about 45.72%, even though its permeance is very low. This observation can originate from the morphology of Cu-PTAPP film which has more rigid and uniform pores. In addition, the rejection performance of the PTAPP membrane using a 0.5 mM concentration of TAPP monomer accounts for 29.54%, lower than that using a 1.0 mM concentration (**Figure 4.13(c)**). This given values are consistent with literature that in theoretical consideration, the higher concentration in performed electropolymerization greatly increases the mass deposition and surface area of PTAPP film.

This study further evaluated the membrane performance against dye in water, as shown in **Figure 4.13(e)**. Unexpectedly, compared to the rejection for dye/methanol, the rejection was

decreased by 31%, from 49.05% to 29.54%. Otherwise, the permeance increased with high deviancies, from 5.37 $L.m^{-2}.h^{-1}.bar^{-1}$ to 96.02 $L.m^{-2}.h^{-1}.bar^{-1}$. The decreasing trends of those solvents in pressure-driven process was reported by Zhou et al., (2020). It was observed that the permeance of methanol is superior to ethanol and isopropanol. However, the permeance values in this study were contradictory to the previous works and by following the dynamic viscosity of solvents in **Table 4.1**. The significant errors were contributed by the forming defect while membrane was exposed by organic solvent.

Table 4.1 *The properties of methanol and water*

Solvent	**Viscosity at 25°C**	**Molar Volume** $(V_m, mL.mol^{-1})$	**Density** $(gr.mL^{-1})$	**Surface Energy** $(\gamma, mN.m^{-1})$	**Hansen Solubility Parameters (MPa$^{1/2}$)**		
					δ_m	δ_p	δ_h
Methanol	0.54	40.46	0.79	22.50	15.1	12.3	22.3
Water	0.89	18	1.00	72	15.5	16.0	42.3

On account of the significant difference in top and bottom film morphology, this study thus evaluated their performance (**Figure 4.13(d)**). By placing the bottom surface as the upper layer of the membrane, the rejection and permeance were increased to 59.09% and 7.82 $L.m^{-2}.h^{-1}.bar^{-1}$, respectively. An improvement in separation properties is supported by the bottom film structure, owing to the specific surface area, as depicted in **Figure 4.12**. Moreover, when the bottom film was used, the membrane constructed an asymmetrical structure from highly dense to less pores. Asymmetric membrane using bottom film as the functional layer facilitates the molecular sieving. Thanks to its rigid-structured nanofilm, the large molecular solute, here, RB-5 dye, can be rejected in the upper surface and pore-clogging is minimalized, but still allows solvent permeating through.

The investigation of PTAPP/Nylon membrane, with various well-determined structures through electropolymerization, showed the capabilities in the separation process. Of note, the reported

values in this study yet fulfilled the expectation. The relatively low rejection, in particular, was still under the reported values in literature. Therefore, the further improvement of porphyrinic membrane is crucial considerations.

Table 4.2 *The Reported permeance and dye/solvent rejection values*

Material/ Function	Design/ Method	Permeance	Rejection	Literature
PTAPP/Nylon, NF	Porous Material, CMP, EP	$5.37 - 57.90$ L.m^{-2}.h^{-1}.bar^{-1} (methanol permeance) and 96.02 L.m^{-2}.h^{-1}.bar^{-1} (water permeance)	$29 - 59\%$ (RB-5, 991.8 g mol^{-1})	This Work
PA-Mil-53 or PA-ZIF-8, OSN	MOF, Conventional IP	1.8 ± 0.2 L.m^{-2}.h^{-1}.bar^{-1} (methanol permeance)	-	Sorribas, et al., 2013
Polyamide (PA) NF	Conventional IP	4.5 L.m^{-2}.h^{-1}.bar^{-1} (water permeance)	-	Istirokhatun, 2022
CMP composite membrane, OSN	CMP, spin coating	22 L.m^{-2}.h^{-1}.bar^{-1} (methanol permeance)	$< 90\%$ (Molecular weight, 900 – 200 Da)	Liang, et al., 2022
PDA-CNT support membrane, for OSN	-	$(15{,}000 \pm 0.09)$ L.m^{-2}.h^{-1}.bar^{-1} (methanol permeance)	-	Zhou et al, 2020
PDA-CNT-polycarbazole (PC) membrane, OSN	Porous Material, CMP via EP	28 L.m^{-2}.h^{-1}.bar^{-1} (methanol permeance)	$15 - 99\%$ (Molecular weight, 700 – 300 Da)	Zhou et al, 2020
TCTA-EP Membrane, OSN	Porous Material, CMP, EP	33.1 ± 1.2 L.m^{-2}.h^{-1}.bar^{-1} (dimethylformamide, DMF, permeance)	$94.4 \pm 2.2\%$ (Allura Red AC, 496.42 g mol^{-1})	Lu, Liu, Wang, and Zhang, 2022

Material/ Function	Design/ Method	Permeance	Rejection	Literature
PPN membrane	Porous material, Aromatic PPNs	4.57 – 7.10 $L.m^{-2}.h^{-1}.bar^{-1}$ (methanol permeance)	98.6 – 99.1% (Brilliant Blue, BB)	Wang et al., 2020

4.1.6 Ion Salt Separation

Based on the observation of conductivity probes, as shown in **Figure 4.14**, the conductivity in the filtrate chamber performed by PTAPP/Nylon membrane slightly increased in micron-siemens/cm, indicating better rejection. Conversely, Nylon, a single layer only, had a great increase in conductivity in milli-siemens /cm because of its microporous structure.

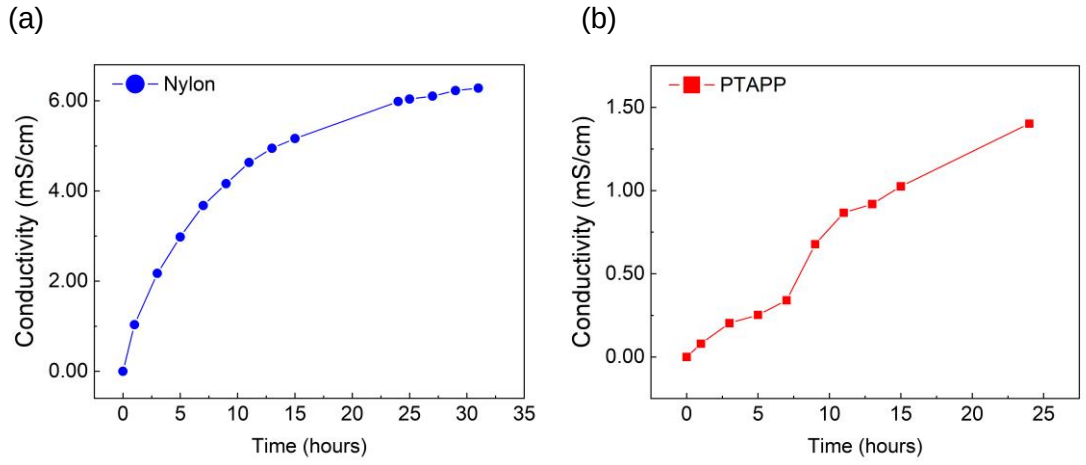

Figure 4.14 Conductivity probe of (a) Nylon membrane and (a) PTAPP/Nylon membrane, using bottom film as the upper layer, against NaCl, 0.1 M, after 24-hour observation in static diffusion cell

Mass transport of salt molecules is influenced by diffusion phenomena as as a result of concentration gradient. In principle, when two liquids with different concentrations are kept together in between semipermeable membrane, the liquid particles naturally move and diffuse through the membrane from area of high concentration to low concentration. The diffusion process continues until the concentration of two liquids is homogenous, and this is called equilibrium. This concept strongly relates to the work presented in this study. As shown in **Figure 4.14(a)**, the conductivity, in filtrate chamber, was greatly increasing in the first two hours, and then an increment became slower and slower with time. At duration of 24 - 30 hour, the increment was insignificant, indicating that the system had reached equilibrium, and the concentration of the two compartments was equivalent.

Besides the difference in concentration, the rate of diffusion is also influenced by the diffusion coefficient of the dissolved substance. In this regard, this study attempted to prove the importance of diffusivity through analytical calculation, provided in **Appendix A**. The calculated diffusion coefficient for Nylon membrane against NaCl is $1.10 \times 10^{-5}\ cm^2/sec$, which has a same order of magnitude with the literature values of $1.99 \times 10^{-5}\ cm^2/sec$ for NaCl electrolyte (UKessays, 2017). This value lies in range of diffusion in liquid, which is $10^{-5}\ cm^2/sec$ (Cassler, 2009). As the diffusion coefficient is verified, the calculated flux is $6.15 \times 10^{-7}\ mol/(sec.cm^2)$.

In contrast, it was unclear that the system was complete for PTAPP/Nylon membranes because of the slow diffusion rate. The result, as shown in **Figure 4.14(b)** indicated that the electropolymerized PTAPP membrane has dense pores at nanoscales, superior to the control membrane. Due to the rigid framework of the bottom PTAPP film, the movement of salt molecules from the feed to the filtrate chamber was slowed down.

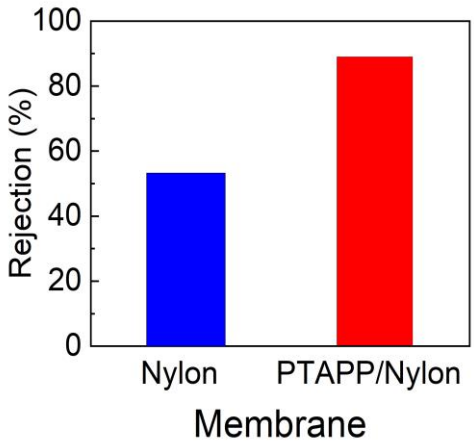

Figure 4.15 *Rejection performance of Nylon membrane and PTAPP/Nylon membrane using bottom film as the upper layer, against NaCl, 0.1 M, after 24-hour observation in static diffusion cell*

To extend this observation, the rejection values were derived from the conversion of conductivity to concentration which was previously recorded in the conductivity probe in **Appendix A**. PTAPP/Nylon membrane exhibited 89% rejection higher than Nylon membrane (53%), as depicted in **Figure 4.14**. The high rejection value of the PTAPP membrane indicated that PTAPP is a proven polymer film effective as a selective layer in salt separation.

4.1.7 Molecular-sieving Selectivity

This investigation proved the ability of PTAPP membrane to separate dye molecules based on molecular size. The separation of dye mixtures is shown in digital photo of the diffusion cell (**Figure 4.16**). It was proven that the PTAPP/PE membrane showed a response to the varying molecular weight of dyes. As shown in digital photo in **Figure 4.16(a)**, after 24-hour mixing, small portion of CR dye was separated from the feed solution. In contrast, the filtration turned slightly red, and no blue color was visibly detected in filtrate chamber, indicating that the selectivity diffusion permitted CR dye only.

(a)

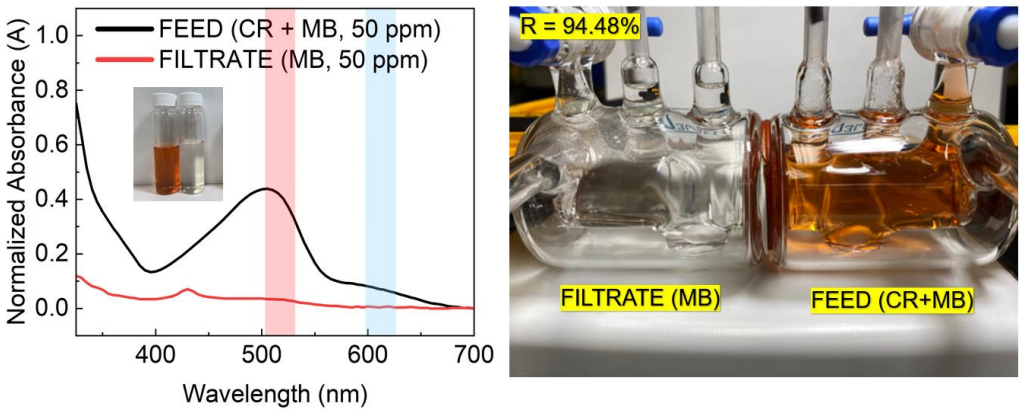

(b)

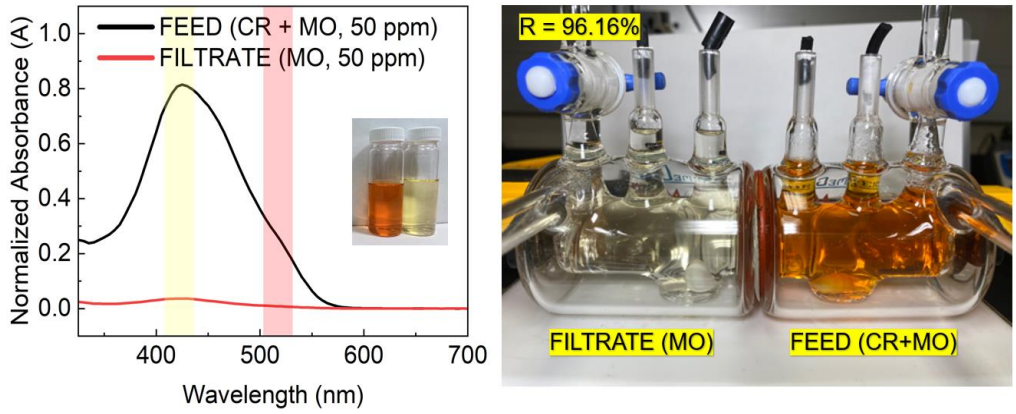

Figure 4.16 *The UV-Vis spectra and digital photographic images of PTAPP/Nylon membrane, using bottom film as the upper layer, against (a) mixed solution of Congo Red (CR) and Methyl Blue (MB), 50 ppm, in methanol and (a) mixed solution of Congo Red (CR) and Methyl Orange (MO), 50 ppm, in methanol*

The visualization of dye separation in diffusion cell was also performed with the mixture of CR and MO, as shown in in **Figure 4.16(b)**. In the first two hours, the filtrate solution turned slightly yellow, and then the color turned more yellow after 24 hours. The rapid transport of MO dye molecule, instead of CR, through PTAPP/PE membrane was promoted by its smaller molecular weight. The rejection values were obtained by measuring the absorption of both feed and filtrate solution using UV-Vis spectra measurement. The rejections about 94.48% and 96.16% were attributed to the dye separation of CR and MB, and the dye separation of CR and MO, respectively.

4.2 Tri-layer PTAPP Membrane

Of all the demonstrated work in bi-layer membranes, the permeable and defect-free membrane is a huge challenge in the electropolymerization and free-standing film process. Moreover, the weak adhesion of PTAPP film and the porous support material potentially leads the film on top to delaminate. Hence, in this work, the fabrication of tri-layer PTAPP membrane is oriented to in-situ electrodeposition adopting conductive material on a porous substrate.

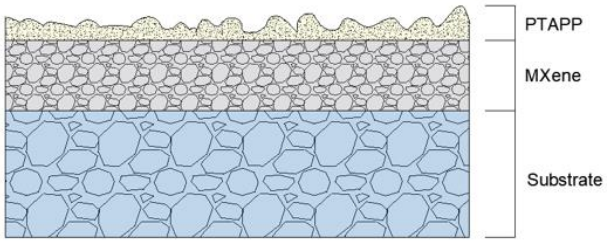

Figure 4.17 *Tri-Layer PTAPP membrane exploiting MXene as an interlayer and conductive material for building porous PTAPP film*

4.2.1 Electropolymerization of PTAPP film on MXene Membrane

Similar to the electropolymerization mechanism of PTAPP film on ITO substrate, TAPP monomers were electropolymerized on the as-prepared porous support consisting of MXene and substrate layer. Here, for the first time, MXene was used as the conductive material to build the conjugated microporous material and simultaneously as an interlayer; therefore, the free-standing film is no longer necessary. Owing to the outstanding conductivity, surface chemistry tunability, and excellent mechanical properties (Ling, et al., 2014), MXene is a promising candidate for interlayer like CNT reported by Zhou's group (2020) and Lu's group (2022).

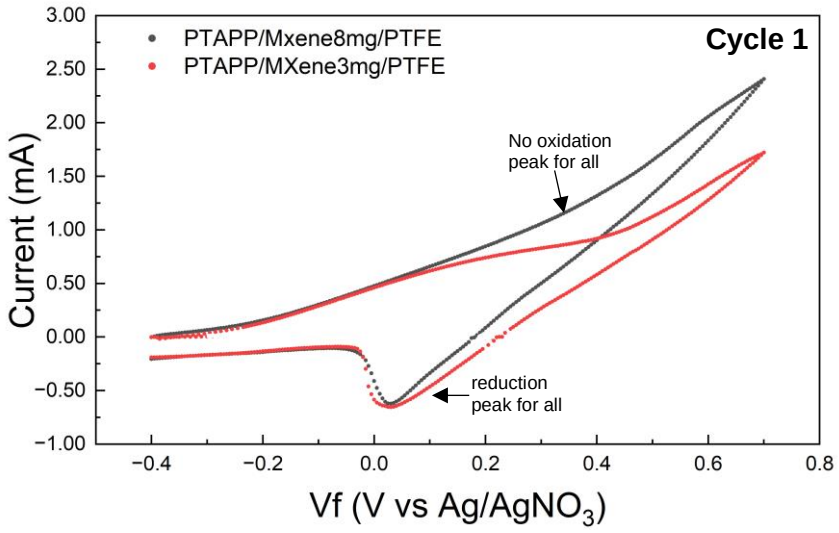

Figure 4.18 *Cyclic voltammogram of electropolymerized PTAPP film on MXene/PTFE membrane using 3-mg and 8 mg MXene mass loading and scan rate of 10 mV/s through 10 cycles, performed in 0.5 mM TAPP monomer in DCM, 0.05 M TBAPF6, and 5% v/v pyridine solution*

The electropolymerization mechanism of PTAPP on MXene surface using 8 mg mass loading exhibited a higher current in the anodic region, indicating the forming film is thin because less monomer reacts at working electrode surface. In contrast, even though the electropolymerization using 3 mg mass loading of MXene has a similar shape to that using 8 mg mass loading of MXene, the resulting current is lower. The significant difference in color between two electropolymerized PTAPP films on MXene is shown in **Figure 4.19**. Mass loading of 8 mg performed darker blue color while the other was brown. After all, the optimal mass loading of MXene for electropolymerization has yet to be drawn, and the permeation test is considerable to confirm it further.

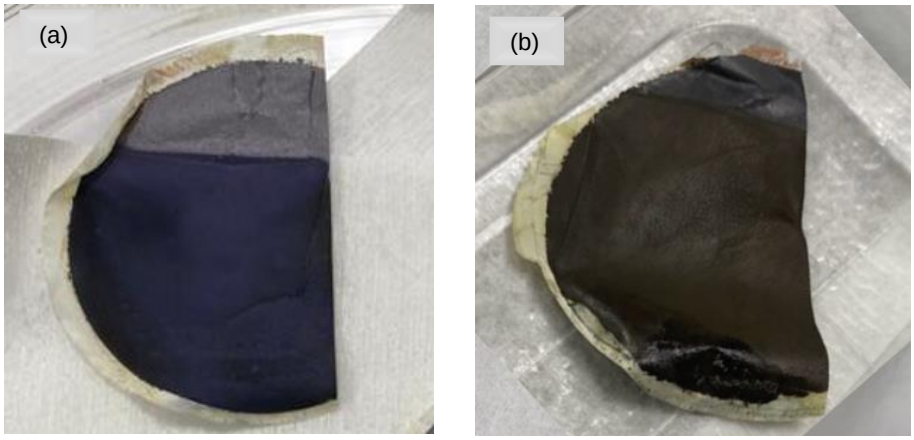

Figure 4.19 *Digital photographic images of electropolymerized PTAPP film on MXene/PTFE membrane using (a) 8 mg and (b) 3-mg MXene mass loading and scan rate of 10 mV/s through 10 cycles, performed in 0.5 mM TAPP monomer in DCM, 0.05 M TBAPF6, and 5% v/v pyridine solution*

The second investigation was electrochemically conducting PTAPP film using various scan rates. As shown in **Figure 4.20**, the resulting currents decrease as the potential scan rate rises, which is relevant to the theory and the experimental works discussed in **sub-section 4.1.1**. However, there is an unknown reason for the absence of oxidation peaks, while slight reduction peaks were observed in the cyclic voltammogram. In fact, the PTAPP was successfully deposited on MXene for scan rates of 5 mV/s, 10 mV/s, and 15 mV/s, indicated by the dark color in an electropolymerized area of the MXene surface.

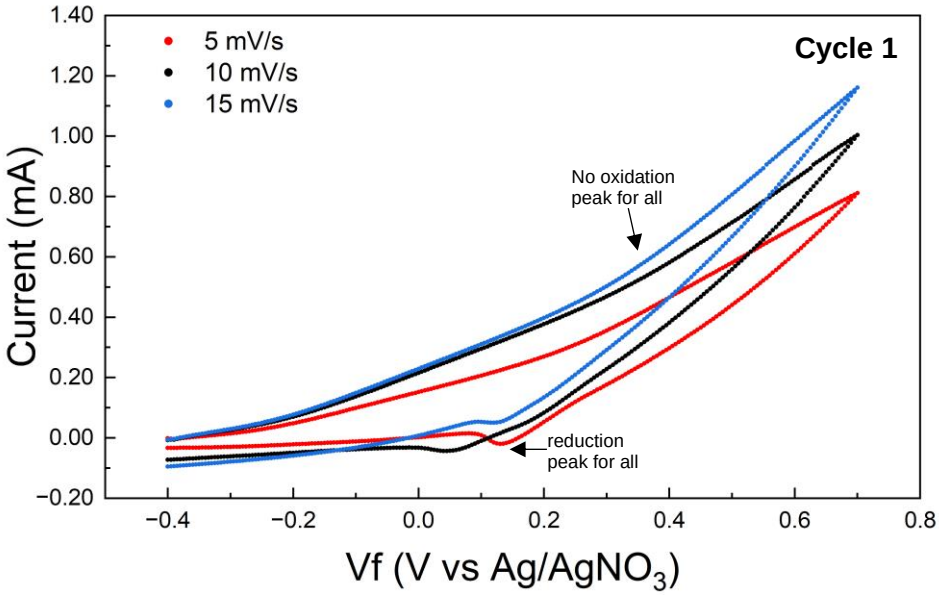

Figure 4.20 *Cyclic voltammogram of electropolymerized PTAPP film on MXene/PTFE membrane, with 8 mg mass loading of MXene using scan rates through 10 cycles, performed in 0.5 mM TAPP monomer in DCM, 0.05 M TBAPF6, and 5% v/v pyridine solution*

The tendency of MXene layer to delaminate when it is exposed to the solution during electropolymerization is a crucial consideration. This issue is possibly due to the weak adhesion with porous substrate or weak adhesion with MXene flakes themselves. Hence, the observation was continued by electrochemically polymerizing PTAPP film on MXene using different porous support, namely Polyethylene (PE) and Polytetrafluoroethylene (PTFE). Both support membranes are hydrophilic.

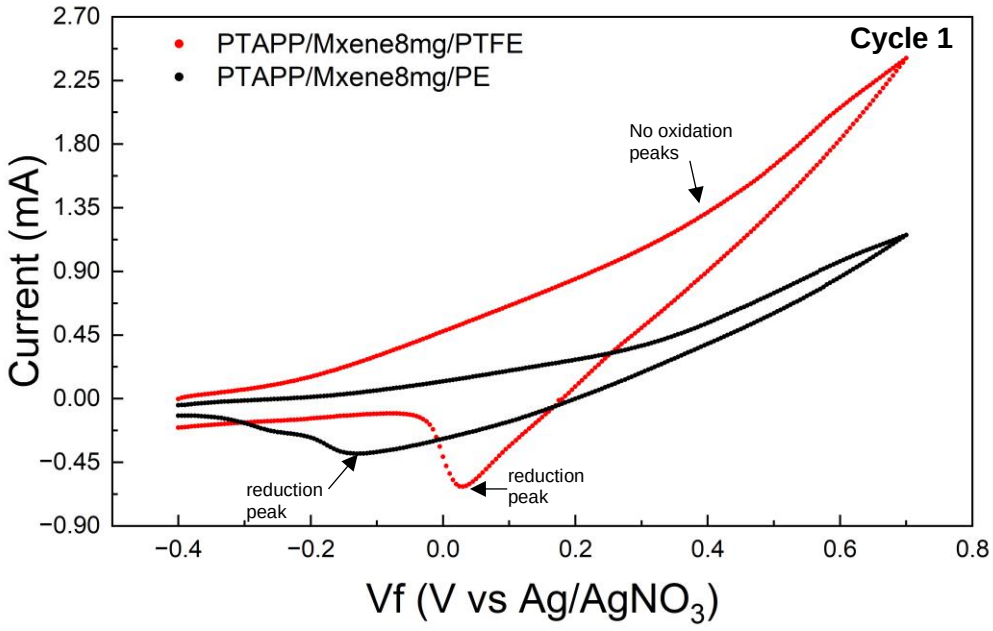

Figure 4.21 *Cyclic voltammogram of electropolymerized PTAPP film on MXene/PTFE and MXene/PE membrane with 8 mg mass loading of MXene using scan rate of 10 mV/s through 10 cycles, performed in 0.5 mM TAPP monomer in DCM, 0.05 M TBAPF6, and 5% v/v pyridine solution*

The cyclic voltammogram of electropolymerized PTAPP on MXene/PTFE and MXene/PE, with fixed processing parameters such as mass loading, showed a huge gap in resulting currents as shown in **Figure 4.21**. It was observed that PTAPP/MXene/PTFE possessed the lower resulting current. Cracking and delamination may occur when the MXene layer on support is immersed in the solution, leading to reduced conductivity. Back to the physical nature of porous support membranes, PE is typically rigid, whereas PTFE, unlaminated, is more flexible. When MXene/PE is immersed in a solution, strong adhesion between MXene, solvent, and porous support takes place, then suddenly porous support bends, not flat, and causes cracking on the MXene layer. However, it is not always the case. In this investigation, the well-deposited films were achieved, as shown in **Figure 4.22,** even though minor damage may still occur.

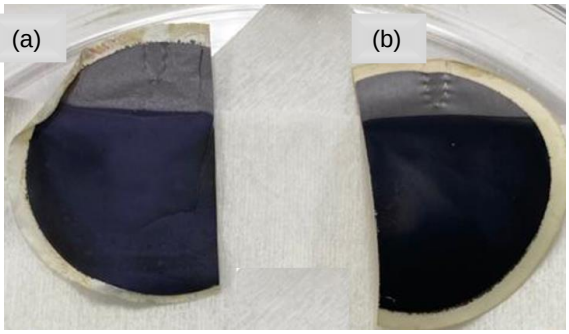

Figure 4.22 *Digital photographic images of electropolymerized PTAPP film on (a) MXene/PTFE membrane and (b) MXene/PE membrane using 8 mg mass loading of MXene and scan rate of 10 mV/s through 10 cycles, performed in 0.5 mM TAPP monomer in DCM, 0.05 M TBAPF6, and 5% v/v pyridine solution*

Solvent has a destructive effect on MXene layer because it swells the MXene flakes and weakens the bonding between them. Hence, electropolymerization by using different solvents was investigated.

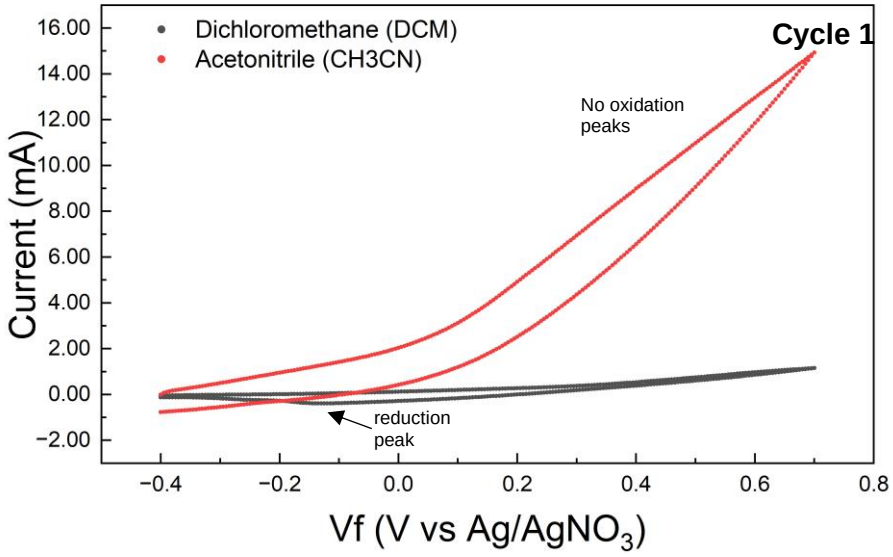

Figure 4.23 *Cyclic voltammogram of electropolymerized PTAPP film on MXene membrane using Dichloromethane (DCM) and Acetonitrile (CH_3CN) solvents, 8 mg mass loading of MXene and scan rate of 10 mV/s through 10 cycles, performed in 0.5 mM TAPP monomer in DCM or CH_3CN, 0.05 M TBAPF6, and 5% v/v pyridine solution*

A huge gap of resulting currents in the CV curve was observed, as shown in **Figure 4.23**. The highest current was contributed by electropolymerization using acetonitrile solvent. When the solid electrode surface was immersed in a solution containing acetonitrile solvent, MXene layer was relatively stable and did not pose any damage. However, no oxidation and reduction were detected in this process, indicating that the film may not be completely formed on the MXene surface. Based on the color, PTAPP/MXene8mg/HDPE using acetonitrile solvent displayed the dark blue color on the MXene surface.

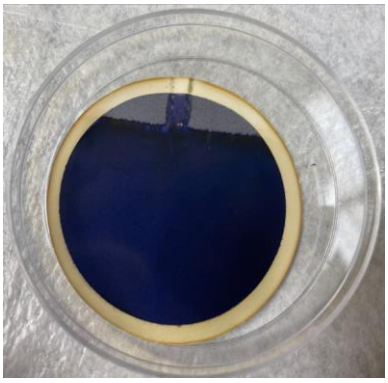

Figure 4.24 *Digital photographic image of electropolymerized PTAPP film on MXene membrane using scan rate of 10 mV/s through 10 cycles, performed in 0.5 mM TAPP monomer in Acetonitrile (CH_3CN), 0.05 M TBAPF6, and 5% v/v pyridine solution*

4.2.2 SEM Characterization

The understanding of PTAPP film growth on suitable porous support by regulating electrodeposition parameters was further discussed using SEM. The uniformity of PTAPP film varies not only on the top surface but also inside the porous MXene layer. This is because MXene porous support network is formed by the deposition of MXene flakes which are a highly conductive and extremely high surface area for PTAPP to grow. It thus suggests that the electropolymerized PTAPP film on MXene/Substrate porous support rendered the highly porous film, but less uniform, compared to the original one on the ITO substrate.

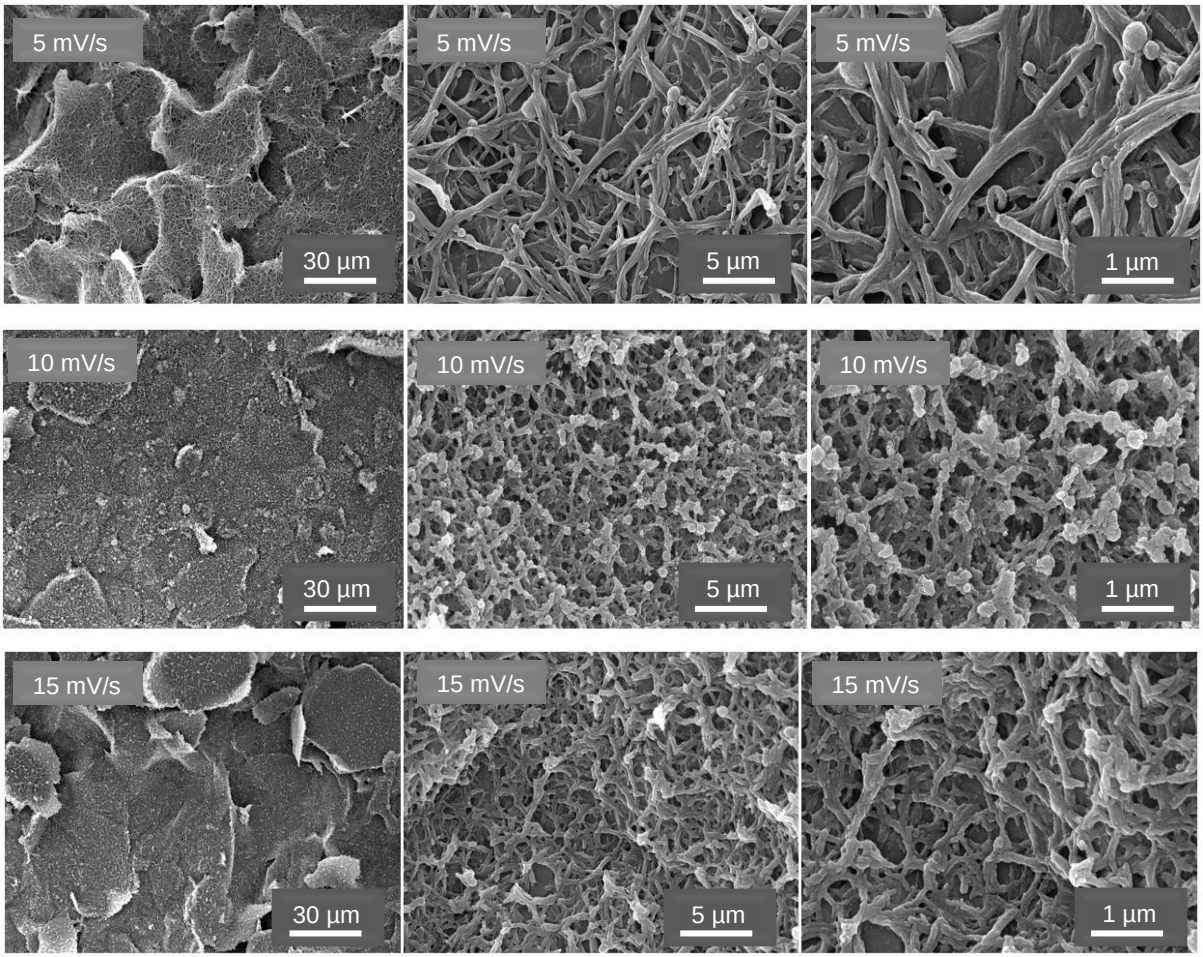

Figure 4.25 *SEM images of electropolymerized PTAPP film morphology on MXene/PTFE membrane, with 8 mg mass loading of MXene using scan rates through 10 cycles, performed in 0.5 mM TAPP monomer in DCM, 0.05 M TBAPF6, and 5% v/v pyridine solution*

Various scan rates were used to investigate the morphology of PTAPP film on pre-deposited support membrane. Theoretically, a lower scan produces a denser and thicker film. However, as shown in the SEM image at 30 µm resolution (**Figure 4.25**), PTAPP film electropolymerized with a scan rate of 5 mV/s did not grow as uniform as that with a scan rate of 10 mV/s and the MXene layer on top surface were rough and has many gaps between flakes. Despite not smoothly covering the entire surface, PTAPP film electropolymerized with 5 mV/s spread out

in a single MXene flake with wider nanofibers, as seen at a higher resolution of 3 µm and 1 µm. Even though the deposition of PTAPP film did not form the expected thickness, it was assumed that the oxidative polymerization might locally take place inside MXene layer. By contrast, the electropolymerization with a scan rate of 10 mV/s on individual MXene flakes showed the fractionization of PTAPP film on the top surface, indicating this film has formed specific thicknesses and mechanical strength from their network. Moreover, its fraction does look like a spherical shape on the top surface instead of a finger-like shape. A similar structure was also observed in electropolymerized PTAPP film using 15 mV/s; however, the crystallization was uniformly covering the MXene layer surface but still forming the fraction on top.

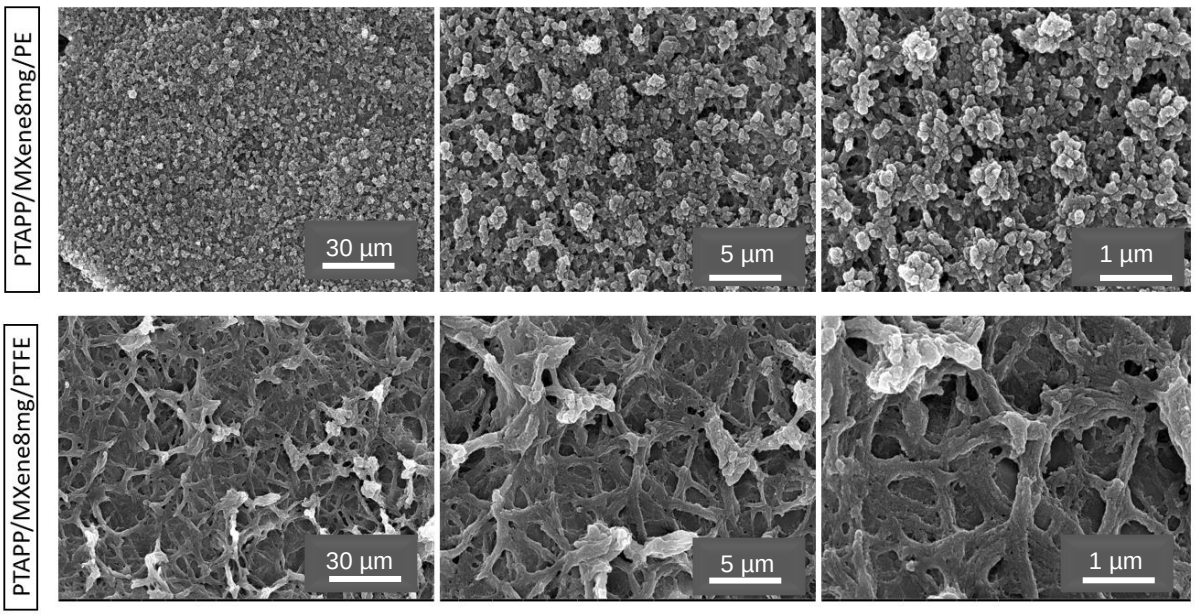

Figure 4.26 *SEM Images of electropolymerized PTAPP film morphology on MXene/PE and MXene/PTFE membrane, with 8 mg mass loading of MXene using scan rates through 10 cycles, performed in 0.5 mM TAPP monomer in DCM, 0.05 M TBAPF6, and 5% v/v pyridine solution*

A spherical shape was also observed in electropolymerized PTAPP film on MXene/PE, which was previously discussed in **sub-section 4.2.1**. Despite the short window resulting currents on CV curve, film growth occurred, but forming somewhat different shape as shown in **Figure 4.26** for PTAPP/MXene8mg/PE. Nonetheless, this film displayed a very high-density level. It was impossible to claim the impurities of the electrolyte solution since PTAPP/MXene8mg/PTFE was also electropolymerized using the same batch and produced the common nanofibrous shape with large diameter.

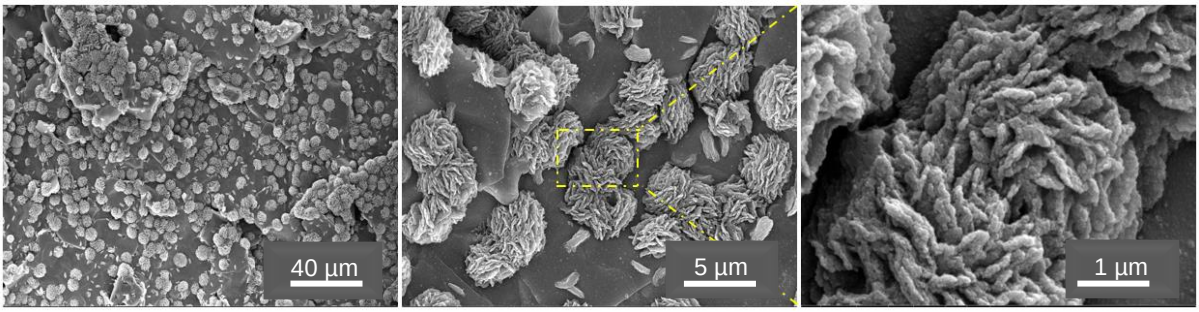

Figure 4.27 *SEM images of electropolymerized PTAPP film morphology on MXene Membrane, with 8 mg mass loading of MXene using scan rates through 10 cycles, performed in 0.5 mM TAPP monomer in Acetonitrile (CH_3CN), 0.05 M TBAPF6, and 5% v/v pyridine solution*

The electropolymerization process was improvised by using acetonitrile in the electrolyte solution, which was previously discussed in **sub-section 4.2.1.** Unexpectedly, the forming PTAPP film was not complete as expected, as shown in **Figure 4.27**. Even though discoloration occurred on MXene layer, SEM confirmed the poor uniformity and the PTAPP structure was more like flower but covering any gaps between MXene flakes on top. The exact cause of this evidence is unknown. Back to the CV curve, depicted in **Figure 4.23**, the oxidation peak was not observed, indicating that transferred electron in coupling reaction may undergo slowly. It was also assumed that acetonitrile as solvent did not dissolve the analyte (TAPP monomer) and the supporting electrolyte (TBAPF6) homogenously in solution.

4.2.3 Dead End Filtration

This study provided several experimental works to understand better the impact of PTAPP film properties using MXene as an interlayer on the separation performance. Tri-layer PTAPP membranes were prepared with various treatments such as membrane supports (PTFE/HDPE/PE), MXene mass loading, and PTFE coatings. In addition, to optimize the function of the MXene layer, here, the synthesis of MXene was done using LiF method instead of HF method to achieve a smooth MXene surface with fewer gaps between flakes. Detailed information for each treatment is provided in **Table 4.3**.

Table 4.3 The Prepared Membranes with Various Treatment

Experiment Code	Structural Membrane	Treatment
A1	PTAPP/MXene8mg/PE	MXene Synthesis via HF
A2	PTAPP/MXene8mg/PE	MXene Synthesis via HF, PTFE coating on PTAPP film via iCVD method
A3	PTAPP/MXene8mg/PTFE	MXene Synthesis via HF
A4	PTAPP/MXene8mg/PTFE	MXene Synthesis via HF, PTFE coating on PTAPP film via iCVD method
B1	PTAPP/MXene3mg/PTFE	MXene Synthesis via HF
C0	MXene2.5mg/HDPE	MXene Synthesis via LiF, no EP coating
C1	PTAPP/MXene2.5mg/HDPE	MXene Synthesis via LiF

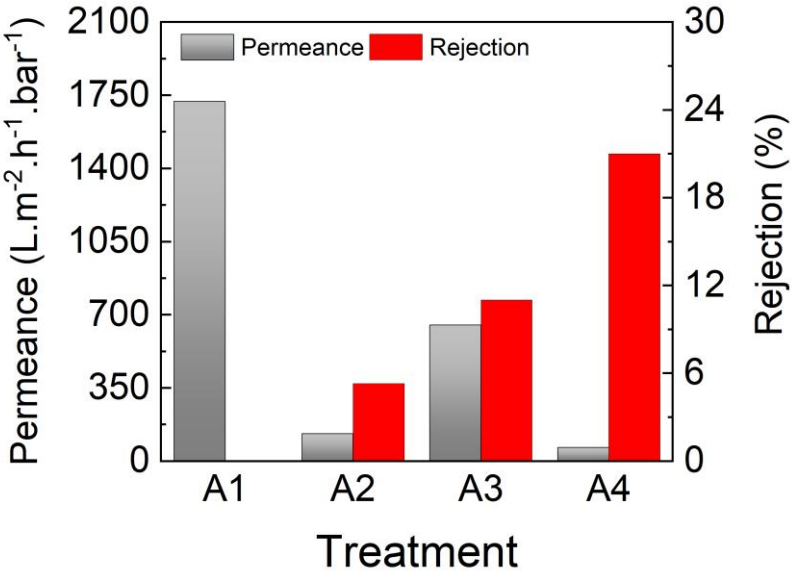

Figure 4.28 *Separation performance of Tri-layer PTAPP membrane using 8 mg MXene mass loading deposited on different porous supports with or without PTFE coating via iCVD, toward Reactive Black -5 (RB-5) dye in methanol at applied pressure 10 psi*

The instability of tri-layer PTAPP membrane results from the vulnerability of the MXene layer to cracking or having a defect when pressure is applied in the separation process. Since the defect exists, the selective PTAPP film has lost its function to filter. Indications of defects are no or fewer molecules rejected and too large a permeance value. As shown in **Figure 4.28**, using MXene/PE as a porous support membrane for PTAPP growth **(A1)** demonstrated the zero value of rejection and the permeance of 1720 $L.m^{-2}.h^{-1}.bar^{-1}$. In contrast, when the PTAPP film was electrodeposited on MXene/PTFE membrane **(A3)**, the rejection increased by 11%, accompanied by a decrease in the permeance value of 62%, compared to those values of A1, indicating that MXene appeared to be more stable when paired with PTFE.

In attempting to keep the function of PTAPP film as an active layer and minimize the potential defect of MXene layer due to harsh conditions by organic solvent and pressure, PTAPP film was coated with PTFE using iCVD method. The coated PTAPP membranes **(A2 and A3)** showed increased rejection values but lower permeance compared to non-coated PTAPP

membranes **(A1 and A3)**. About 20% rejection and permeance of 45.39 $L.m^{-2}.h^{-1}.bar^{-1}$ were performed by PTAPP film deposited on MXene/PTFE with PTFE coating. Even though the enhancement is insignificant, the coating via iCVD with a small concentration of PTFE helps to shield the PTAPP and MXene layers.

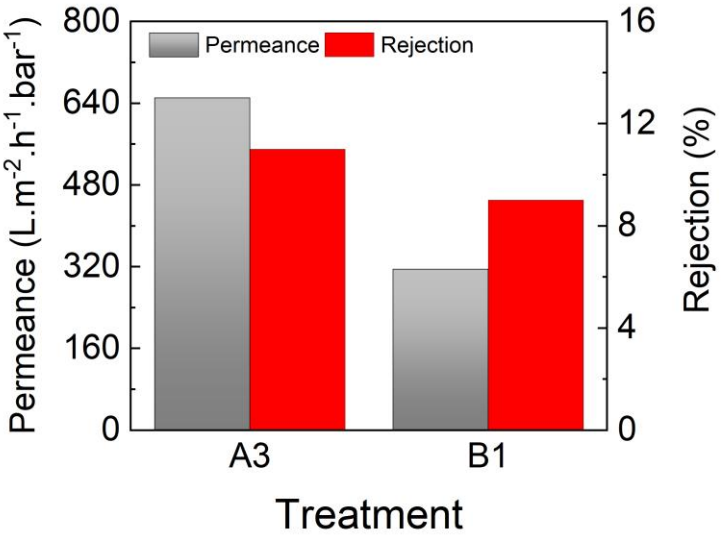

Figure 4.29 *Separation performance of Tri-layer PTAPP membrane using various MXene mass loading (3 and 8 mg) on PTFE, toward Reactive Black-5 (RB-5) dye in methanol at applied pressure 10 psi*

This study investigated using 3 mg and 8 mg mass loading of MXene for electropolymerization of PTAPP film. The mass deposition of MXene on the support membrane determines the growth of PTAPP film during electropolymerization. At this point, the mass deposition is considered as it represents the thickness—the thicker the MXene layer, the lower the flux and permeance values. Unexpectedly, the permeance value of **B1** (PTAPP membrane using 3 mg MXene mass loading) is 315 $L.m^{-2}.h^{-1}.bar^{-1}$ lower than that of **A3**. The defect may exist in MXene layer of both **B1** and **A3**. Nevertheless, their rejection values are insignificantly different, indicating that their PTAPP film structure is identical in surface area and pore uniformity.

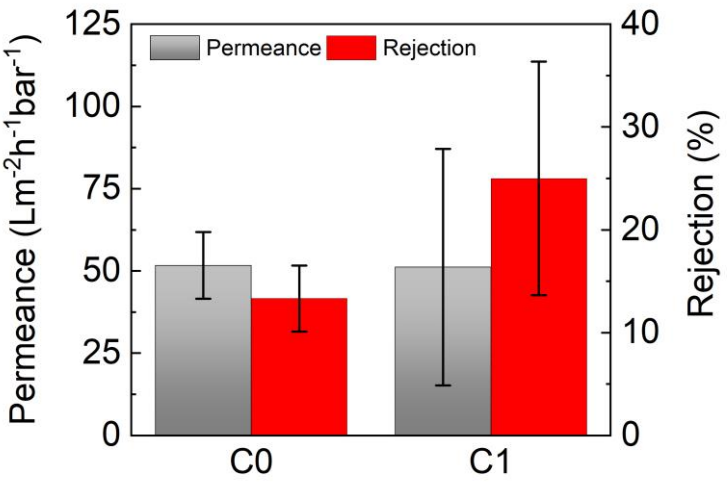

Figure 4.30 *Separation performance of Tri-layer PTAPP Membrane using 2.5 mg MXene mass loading, with the synthesized MXene via LiF, toward Reactive Black-5 (RB-5) dye in methanol at applied pressure 35 psi*

The new MXene flakes prepared via LiF method were deposited on the HDPE membrane, then used as the porous support membrane for PTAPP film. MXene layer is characterized by a smoother surface and reduced gaps, which are ideal for building porous PTAPP film. As shown in **Figure 4.30**, the rejection values of the electropolymerized PTAPP membrane on MXene/HDPE (**C1**) are higher than that of the control (**C0**). After testing three times for each membrane, the permeance values were not significantly different. The rejection was increased from 13% to 25%, showing that the PTAPP film was nicely formed and worked as a selective layer. Variability in terms of permeance and rejection values was observed for PTAPP/MXene2.5 mg (**C1**), shown by a high error bar. These deviancies indicate defects in MXene layer and non-uniform PTAPP growth on MXene surface.

4.3 FT-IR Measurement

The surface chemistry structure of PTAPP film was investigated using Fourier-transform infrared spectroscopy (FTIR). FTIR spectra of electropolymerized PTAPP films was collected using an ALPHA spectrometer from Bruker, then it was compared against FT-IR spectra from literatures. The structural connection of PTAPP consists of diphenylamine, dihydophenazine, and phenazone linkages, which all are detected in the reflectance FTIR (Walter and Wamser, 2010). The region of N-H stretching of both the aminophenyl and the pyrroles is found in peaks around 3330 - 3470 cm^{-1} and 3211 cm^{-1}, respectively. With added pyridine, the peak that suggested phenazine groups is spotted at 820 cm^{-1}.

The peak corresponding to polymers appears as a shoulder around 1630 cm^{-1} (Li, et al, 2014), and it is assigned to the C=C and C=N phenazine ring stretching vibration. The peaks in 1068 cm^{-1} and 1087 cm cm^{-1} are attributed to C-H deformation modes in phenazine-linkage rings (Wang and Wamser, 2014). The distinct phenazine skeletal vibration characterizes a coupling reaction of aminophenyl groups in TAPP molecules at 860 cm^{-1} (Mohammadhi, 2018; Xia et al., 2020).

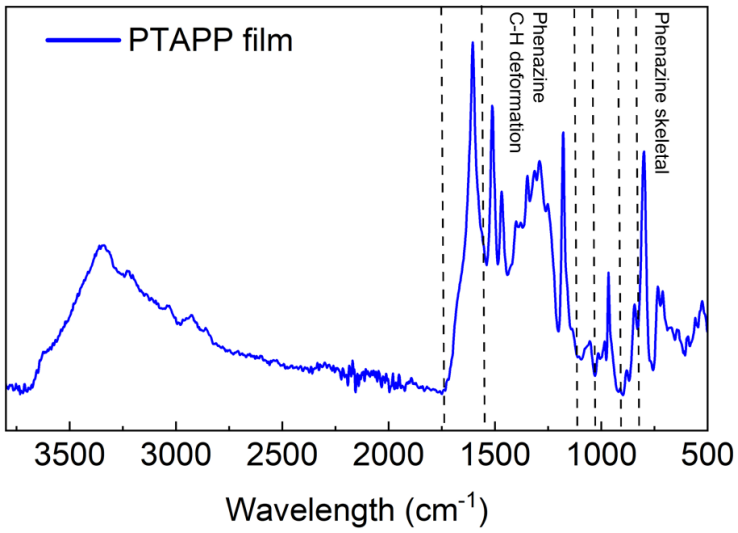

Figure 4.31 FTIR Spectra of electropolymerized PTAPP film (free-standing) using scan rates through 10 cycles, performed in 1.0 mM TAPP monomer in DCM, 0.05 M TBAPF6, and 5% v/v pyridine solution

As shown in **Figure 4.31**, the C=C and C=N phenazine was not observed in FTIR Spectra of free-standing film. The new vibrations of phenazine skeletal were observed at 844 and 881 cm^{-1}. In addition, N-H in terminal aminophenyl groups of PTAPP vibration lies in range of 3208 - 3360 cm^{-1}. The detailed FTIR Spectra is provided in **Table 4.4**.

Table 4.4 *FTIR spectra of electropolymerized PTAPP films*

Vibration Mode	**PTAPP (cm^{-1})**
Disubstituted phenyl-out of plane	799
Phenazine-skeletal vibration	844
Phenazine-skeletal vibration	881
Phenyl ring deformation	985
-C-H deformation phenyl ring	1054
-C-H deformation phenazine ring	1074
Beta pyrrole C-H deformation	1180
Stretching -C-N aromatic amine	1348
C=N phenazine ring	1380
Tetrapyrrole C-C-N-C	1468
Tetrapyrrole C-C-N-C	1513
Amino N-H deformation	1605
C = C stretching (non-conjugated)	1674
Pyrrole N-H stretching	3234
$-NH_2$ Symmetrical	3340
$-NH_2$ Asymmetrical stretching	3362

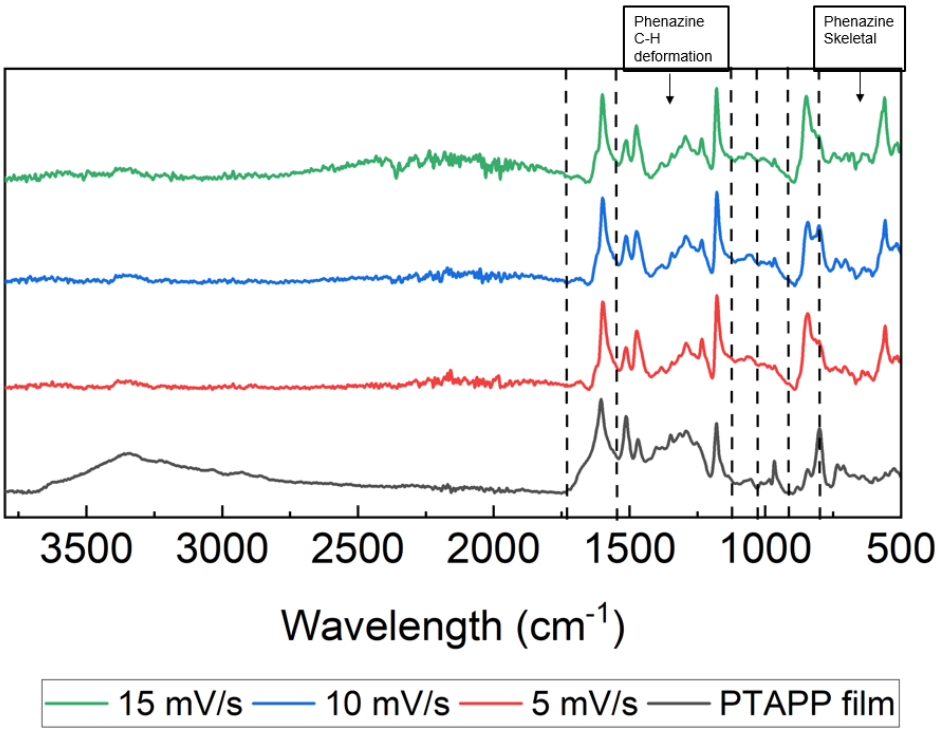

Figure 4.32 *FTIR spectra of electropolymerized PTAPP film on MXene/PTFE using various scan rates through 10 cycles, performed in 0.5 mM TAPP monomer in DCM, 0.05 M TBAPF6, and 5% v/v pyridine solution*

The FTIR Spectra of electropolymerized PTAPP film on pre-deposited support membrane using various scan rates were performed to confirm the deposition of PTAPP film. As shown in **Figure 4.32**, similarities of peaks were observed, and the new vibration at 558 cm^{-1} was attributed to the electrolyte, TBAPF6, that remained in the film. Compared to the FT-IR Spectra of PTAPP film, the vibration modes of N-H in terminal aminophenyl groups of PTAPP, in electropolymerized on MXene, decreased in intensity.

CHAPTER FIVE: CONCLUSION AND FUTURE DIRECTION

5.1 Conclusion

Various progressive efforts have been made to establish novel materials with well-defined structures at sub-1 nm size and great stability for thin-film composite nanofiltration (NF). Herein, the conjugated microporous polymers (CMPs), a sub-class of porous organic polymers, are a breakthrough material due to their highly ordered network, and porphyrin, one of many functional groups, can form conjugated polymers. Ease of reproducibility with simplifying processing is the highlight of porphyrin-based films via electropolymerization.

The investigation of PTAPP membrane was divided into two main sections. The first section was PTAPP film electropolymerized on indium tin oxide (ITO), then the film was transferred on porous support. The second section was PTAPP film electropolymerized on pre-deposited MXene on a porous support. The separation performance of the bilayer PTAPP membrane was focused on permeability and rejection against dye/solvent through dead-end cells. In addition, salt separation and selectivity toward dye/solvent through static diffusion cells were observed. Thus, conclusions from each section including the separation properties and surface morphologies, have been drawn as follows:

1. Scalable scan rates, monomer type, and monomer concentration strongly affect the electropolymerization behavior of PTAPP film on ITO substrate, which is monitored by a cyclic voltammogram (CV) curve.
2. Well-defined thickness of electropolymerized PTAPP film can be successfully obtained by adjusting the scan rates and concentrations, and the PTAPP film is flexibly electropolymerized on ITO glass in multiple sizes without obtaining the defect issues. Hence, this scalable material is a promising candidate for industrial applications.
3. Obtaining the free-standing film with minimum potential defects is a challenge depending on polymerization conditions, such as the impurities of electrolyte solution. Well-electrodeposited film induces spontaneous delamination and produces free-standing films.

4. The morphology of poly-TAPP film, electropolymerized on ITO substrate, is a highly nanofibrous network with varying density depending on the processing parameters. In the presence of metal ions such as Cupper, the film does not possess nanofibers on the surface. The electropolymerization using ITO as substrate produces a dense bottom surface film.
5. Great separation of PTAPP/Nylon membrane using the bottom film as the upper layer of the membrane, accounting for 59% of RB-5 dye rejection in methanol and 7.82 $L.m^{-2}.h^{-1}.bar^{-1}$ methanol permeance. The thickness-formed film by scan rates somewhat presents the non-ordered rejection and permeance. The deviancies were observed during the measurement because of delamination and defect issues.
6. PTAPP/Nylon membrane performed higher NaCl rejection (89%) higher than Nylon membrane only (53%), due to the rigid structure of PTAPP film.
7. Molecular-sieving selectivity against the mixture of two different dyes in methanol is proven, in which the lower molecular weight can permeate easily through the membrane. The rejection values of 94.48% and 96.16% were attributed to the dye separation of CR and MB and the dye separation of CR and MO, respectively.
8. The oxidation or reduction peak is sometimes absent in the cyclic voltammogram, indicating that the film growth on the MXene surface is not optimal.
9. MXene, as a conductive material, builds the highly porous PTAPP film, but the pore uniformity and thickness vary, not strongly correlated with the scan rates. In addition, the PTAPP structure is somewhat different in fixed parameters.
10. The separation performance of PTAPP membranes exploiting MXene as an interlayer have varying pore uniformity and mechanical stability depending on MXene itself and the adhesion between MXene and support membrane.

5.2 Future Direction

Three-layer assembled membrane using conjugated polymer film through electropolymerization has great potential in the membrane separation process, maintaining high permeance and selectivity simultaneously. PTAPP/MXene membrane is superior in energy saving because the permeance is higher with a lower pressure than the bilayer PTAPP membrane. However, the obstacle of this research is mainly because of the lacking understanding of the suitable formula or conditions to construct a three-layer composite membrane using MXene as the interlayer for building selective porous PTAPP films. Therefore, further optimization needs to be done, for example, by reducing the MXene flake sizes. Specific opportunities for the conjugated polymer using porphyrin as the functional block are the evaluation of membrane testing performance in terms of permeability, selectivity, antifouling capacity, and chemical stability under harsh conditions.

5.3 Porphyrin-containing CMPs Application

The uniqueness of this polymeric material is its tunable properties, especially porosity, which leads to increasing size-sieving with high permeance but does not drastically reduce selectivity. In addition, the membranes are designed with ease of scale-up fabrication, chemical stability, and thermal stability, which are promising for broad challenging environments. The membranes thus offer environmentally friendly energy, low cost, and long life. Due to all these advantages, PTAPP-based films of Conjugated Microporous Polymers (CMPs) are applicable for Nanofiltration membranes, where their function is more devoted to molecular sieving and chemical-stable organic solvent separation. Therefore, this design has the potential to revolutionize its applicability in a wide range of industrial applications, such as wastewater treatment for dye separation and desalination processes.

REFERENCES

Bidhendi G.N, and Nasrabadi, T. (2006). Use of nanofiltration for concentration and demineralization in the dairy industry. *Pakistan Journal of Biological Sciences, 9, p. 991-994*. https://dx.doi.org/10.3923/pjbs.2006.991.994

Bylund, G. (1995). Dairy processing handbook. *Tetra Pak Processing System, Lund, Sweden*.

Cando, A.P., Enriquez, I.R., Tausch, M., and Scherf, U. (2019). Thin Functional Polymer Films by electropolymerization. *Nanomaterials (Basel), 9*. https://doi.org/10.3390%2Fnano9081125

Cassler E.L. (2009). Diffusion Mass Transfer in Fluid Systems. Third Edition. *Cambridge University Press.*

Chen, J., Zhu, Y., and Kaskel, S. (2021). Porphyrin-based metal–organic frameworks for biomedical. *Angewandte International Edition Chemie, Vol. 60, p. 5010– 5035*. http://dx.doi.org/10.1002/anie.201909880

Das et al. (2017). Porous organic materials: strategic design and structure−function correlation. *Chemical Review, 113, p. 1515 – 1563*. https://doi.org/10.1021/acs.chemrev.6b00439

Dawson, R., Cooper, A.I, and Adams, D.J. (2012). Nanoporous organic polymer networks. *Polymer in Science, 37, p. 530 - 563*. https://doi.org/10.1016/j.progpolymsci.2011.09.002

Dai, R., Li, J., Wang, Zhiwei. (2020). Constructing interlayer to tailor structure and performance of thin-film composite polyamide membranes: A review. *Advance in colloid and Interface Science, 282*. https://doi.org/10.1016/j.cis.2020.102204

Dey et al. (2017). Selective molecular separation by interfacially crystallized covalent organic framework thin films. *Journal of the American Chemical Society, 139, 37, P. 13083 – 13091.* https://doi.org/10.1021/jacs.7b06640

Elgrishi et al. (2018). A practical beginner's guide to cyclic voltammetry. *Journal of Chemical Education, 95, p. 197 – 206*. http://dx.doi.org/10.1021/acs.jchemed.7b00361

Fomo et al. (2019). Electrochemical polymerization. *Functional Polymer, p. 105 – 131.* http://dx.doi.org/10.1007/978-3-319-95987-0_3

Freund, L. B., and Suresh, S. (2003). Thin film materials: stress, defect formation and surface evolution. *Cambridge University Press*

Gong, et al. (2019). New insights into the role of an interlayer for the fabrication of highly selective and permeable thin-film composite nanofiltration membrane. *Applied Material and Interfaces, 11, p. 7349 – 7356*. https://doi.org/10.1021/acsami.8b18719

Gottfried, J.M. (2015). Surface chemistry of porphyrin and phthalocyanines. *Surface Science Report, Vol. 70, p. 259-379*. https://doi.org/10.1016/j.surfrep.2015.04.001

Istirokhatun et al. (2022). Ag-based nanocapsule-regulated interfacial polymerization enables synchronous nanostructure towards high-performance nanofiltration membrane for sustainable water remediation. *Journal of Membrane Science, 645*. https://doi.org/10.1016/j.memsci.2021.120196

Jiang et al. (2007). Conjugated microporous poly(aryleneethynylene) networks. *Angew Chemistry International Edition*, 46. https://doi.org/10.1002/anie.200701595

Karan S., Jiang, Z.W, and Livingston, A.G. (2015). Sub-10 nm polyamide nanofilms with ultrafast solvent transport for molecular separation. Science, 348*, p. 1347-1351*, 10.1126/science.aaa5058

Kattula et al. (2015). Designing ultrathin film composite membranes: the impact of a gutter layer. *Scientific Reports, 5*. https://www.nature.com/articles/srep15016

Kral, V., Kralova, J., Kaplanek, R., and Briza, T. (2006). Que vadis porphyrin chemisty. Physiological Research. *Academy of Sciences of the Czech Republic, Prague. Czech Republic.*

Li et al. (2019). Covalent organic frameworks (COFs)-incorporated thin film nanocomposite (TFN) membranes for high-flux organic solvent nanofiltration (OSN). *Journal of Membrane Science, 572, p. 520-531*. https://doi.org/10.1016/j.memsci.2018.11.005

Li et al. (2019). Controllable and rapid synthesis of conjugated microporous polymer membranes via interfacial polymerization for ultrafast molecular separation. *Chemistry of Material, 33, 17, p. 7047-7056*. https://doi.org/10.1021/acs.chemmater.1c02143

Liang, et al. (2018). Microporous membranes comprising conjugated polymers with rigid backbones enable ultrafast organic-solvent nanofiltration. *Nature Chemistry, 10, p. 961 – 967*. https://www.nature.com/articles/s41557-018-0093-9

Ling, et al. (2014). Flexible and conductive MXene films and nanocomposites with high capacitance. *PNAS, 111*. https://doi.org/10.1073/pnas.1414215111

Liu, T, and Liu, G. (2020). Porous organic materials offer vast future opportunities. *Nature Communications, 11*. https://doi.org/10.1038/s41467-020-15911-8

Li, X., et al. (2014). Role of HF in oxygen removal from carbon nanotubes: implications for high performance carbon electronics. *Nano Letters, 14, p. 6179 - 6184*. https://doi.org/10.1021/nl502401c

Lu, Y., Liu W., Liu J., Li, X., Zhang, S. (2021). A review on 2D porous organic polymers for membrane-based separations: Processing and engineering of transport channels. *Advanced Membranes*, 1. https://doi.org/10.1016/j.advmem.2021.100014

Lu, Y., Lie, W., Wang, K., Zhang, S. (2022). Electropolymerized thin films with a microporous architecture enabling molecular sieving in harsh organic solvents under high temperature. *Nature Communication, 11*. https://doi.org/10.1039/d2ta02178a

Meng, Z. and Mirica, K.A. (2020). Covalent organic frameworks as multifunctional materials for chemical detection. Chemical Society Review, 50. https://doi.org/10.1039/D1CS00600B

Michael et al. (2016). Metal-organic frameworks for membrane-based separations. *Nature Reviews Material, 1*. https://www.nature.com/articles/natrevmats201678

Mohammadi Ghaleni, M., et al. (2018). Fabrication of Janus membranes for desalination of oil-contaminated saline water. *ACS Applied Materials & Interfaces, 10, p. 44871 - 44879*. https://doi.org/10.1021/acsami.8b16621

Muller, P. (1994). Glossary of terms used in physical organic chemistry (IUPAC Recommendation 1994). *Pure and Applied Chemistry, 66, p. 1077 – 1184*. https://doi.org/10.1351/pac199466051077

Rajasree, S.S., Li, X. and Deria, P. (2021). Physical properties of porphyrin-based crystalline metal-organic framework. *Communication Chemistry, 4*. https://doi.org/10.1038/s42004-021-00484-4

Skorjanc, T, Shetty, D. and Valan, M. (2021). Covalent organic polymers and frameworks for fluorescence-based sensors. *ACS Sensor, 6, p. 1461 – 1481*. https://doi.org/10.1021/acssensors.1c00183

Sorribash et al. (2013). High flux thin film nanocomposite membranes based on metal–organic frameworks for organic solvent nanofiltration. *Journal of the American society, 135, p. 15201 – 15208*. https://doi.org/10.1021/ja407665w

Stadermann, et al. (2015). Fabrication of large-area free-standing ultrathin polymer films. *Journal of Visualized Experiments*. http://dx.doi.org/10.3791/52832

Sun, et al. (2021). Interlayered forward osmosis membranes with Ti_3C_2Tx MXene and carbon canotubes for enhanced municipal wastewater concentration. *Environmental Science Technology, 55*. https://doi.org/10.1021/acs.est.1c01968

Suresh and Freund. (2003). Thin film material: stress, defect formation and surface evolution. *Cambridge University Press.*

Tashvigh A.A., and Benes, N.E. (2022). Covalent organic polymers for aqueous and organic solvent nanofiltration. *Separation and Purification Technology, Vol. 298*. http://dx.doi.org/10.1016/j.seppur.2022.121589

Ukessays. (2017). Experiment: diffusion coefficient of NaCl in water. Available at: https://www.ukessays.com/essays/chemistry/experiment-diffusion-coefficient-nacl-2563.php

Walter, M.G, and Wamser, C.C. (2010). Synthesis and characterization of electropolymerized nanostructured aminophenylporphryin films. *Journal of Physical Chemistry, 114, p. 7563 - 7574*. https://doi.org/10.1021/jp910016h

Wang, et al. (2020). Aromatic porous polymer network membranes for organic solvent nanofiltration under extreme conditions. *Journal of Materials Chemistry A*. https://doi.org/10.1039/c9ta10190j

Wang, C. and C.C. Wamser. (2014). Hyperporphyrin effects in the spectroscopy of protonated porphyrins with 4-aminophenyl and 4-pyridyl meso substituents. *The Journal of Physical Chemistry A, 118, p. 3605 - 3615*. https://doi.org/10.1021/jp501398g

Wang et al. (2020). Covalent organic frameworks for separation application. *Chemical Society Review, 49*. https://doi.org/10.1039/C9CS00827F

Weder C. Hole control in microporous polymers. *Angew Chemisty International Edition, Vol. 47*. https://doi.org/10.1002/anie.200704697

Xia, L., et al. (2020). Enhanced photodynamic therapy through supramolecular photosensitizers with an adamantyl-functionalized porphyrin and a cyclodextrin dimer. *Chemical Communications, 56, p. 11134 - 11137*. https://doi.org/10.1039/D0CC03574B

Xiang et al. (2021). Systematic tuning and multifunctionalization of covalent organic polymer for enhanced carbon capture. *Journal of American Chemical Society, 137, p. 13301 – 13307*. https://doi.org/10.1021/jacs.5b06266

Xue et al. (2022). Thin-film composite membranes with a hybrid dimensional titania interlayer for ultra-permeable nanofiltration. *Nano Letters, 22, p. 1039 – 1046*. https://doi.org/10.1021/acs.nanolett.1c04000

Yan et al. (2016). Improving the water permeability and antifouling property of thin-film composite polyamide nanofiltration membrane by modifying the active layer with triethanolamine. *Journal of Membrane Science, 513, p. 108 – 116*. https://doi.org/10.1016/j.memsci.2016.04.049

Yang et al. (2020). Mechanistic insights into the role of polydopamine interlayer toward improved separation performance of polyamide nanofiltration membranes. *Environmental Science and Technology, 54*. https://doi.org/10.1021/acs.est.0c03589

Zhang, et al. (2020). Porous organic polymers: a promising platform for efficient photocatalysis. *Material Chemistry Frontier, 4*. https://doi.org/10.1039/C9QM00633H

Zhang, et al. (2022). Tunable organic solvent nanofiltration in self-assembled membranes at the sub-1 nm scale. *Science Advances, 8*. https://doi.org/10.1126/sciadv.abm5899

Zhao, et al. (2021). Enhance water permeance of a polyamide thin-film composite nanofiltration with a metal-organic framework interlayer. *Journal of Membrane Science, 625*. https://doi.org/10.1016/j.memsci.2021.119154

Zhou, et al. (2018). High-performance thin-film composite membrane with an ultrathin spray-coated carbon nanotube interlayer. *Environmental Science and Technology Letters, 5, p. 243 - 248.* https://doi.org/10.1021/acs.estlett.8b00169

Zhou et al. (2020). Electropolymerization of robust conjugated microporous polymer membranes for rapid solvent transport and narrow molecular sieving. *Nature Communications, 11*. https://www.nature.com/articles/s41467-020-19182-1

Zhou et al. (2021). Precise sub-angstrom separation using conjugated microporous polymer membranes. *ACS Nano, 15, 7, p. 11970 – 11980*. https://pubs.acs.org/doi/10.1021/acsnano.1c03194

APPENDIX A

Conductivity Probe: NaCl Concentration versus Conductivity

Concentration	Conductivity Measurement (mS)			Average
	1	2	3	
1 M	100.2	106.3	99.3	101.93
0.9 M	94.00	94.63	92.73	93.78
0.8 M	84.19	84.30	83.95	84.15
0.7 M	77.3	77.79	78.35	77.81
0.6 M	68.42	67.26	68.05	67.91
0.5 M	59.38	59.51	59.20	59.36
0.4 M	47.74	48.06	48.13	47.98
0.3 M	34.33	34.39	34.26	34.33
0.2 M	25.75	25.92	25.98	25.88
0.1 M	13.90	13.89	13.92	13.90
50 mM	7.92	7.906	7.89	7.91
10 mM	1.98	1.96	1.96	1.96
5 mM	0.99	1.00	1.00	0.99

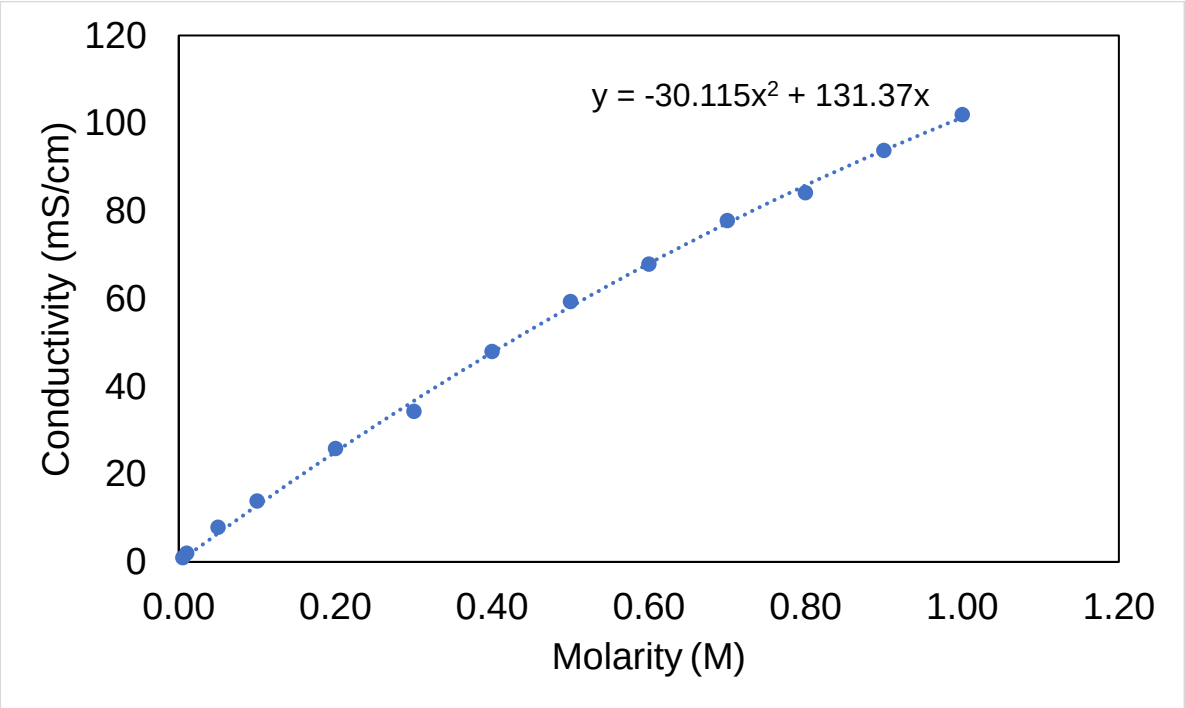

Conversion of Conductivity to Concentration

$$y = -30.115x^2 + 131.27x$$

Where:

Y is conductivity values in milli siemens per cm (mS/cm)

X is concentration in molarity (M)

The conductivity of solution in feed and permeate chamber is known, therefore, the NaCl concentration is tabulated in the below table.

Nylon Membrane versus NaCl solution, 0.1 M

Duration (hour)	Conductivity (mS/cm)		C_{feed} (M)	$C_{p,d}$ (M)
	Feed	Permeate		
0	13.25	0	0.103	0.000
1		1.033		0.008
3		2.172		0.017
5		2.981		0.023
7		3.678		0.028
9		4.161		0.032
11		4.633		0.036
13		4.948		0.038
15		5.164		0.040
24		5.985		0.046
27		6.105		0.047
29		6.227		0.048
31	7.099	6.283	0.055	0.048

PTAPP/Nylon Membrane versus NaCl solution, 0.1 M

Duration (hour)	Conductivity (mS/cm)		C_{feed} (M)	$C_{p,d}$ (M)
	Feed	Permeate		
0	13.25	0.000	0.103	0.000
1		0.079		0.001
3		0.203		0.002
5		0.252		0.002
7		0.341		0.003
9		0.678		0.005
11		0.866		0.007
13		0.918		0.007
15		1.025		0.008
24		1.402		0.011

Salt Rejection

Nylon Membrane versus NaCl solution, 0.1 M

$$\%\ Rejection = \frac{C_{feed} - C_{permeate}}{C_{feed}} \times 100 = \frac{0.103 - 0.048}{0.103} \times 100 = 53\%$$

PTAPP/Nylon Membrane versus NaCl solution, 0.1 M

$$\%\ Rejection = \frac{C_{feed} - C_{permeate}}{C_{feed}} \times 100 = \frac{0.103 - 0.011}{0.103} \times 100 = 89\%$$

Diffusion Coefficient

V_{Feed}	22	ml = cubic cm
$V_{Permeate}$	22	ml = cubic cm (It is assumed constant)
d	0.75	inch
A	0.442	inch square
	2.84	cm square
l	0.016	cm (from measurement using SEM)
H	0.14	coefficient for total area open for diffusion
t	111600	seconds

PROPERTIES

material	Nylon membrane plain filter white filter
sterility	non-sterile
feature	hydrophilic
manufacturer/tradename	Millipore
parameter	100 °C max. temp. (curling may be seen at temperatures above 75°C)
filter diam.	47 mm
thickness	55 µm
pore size	14 % porosity 20.0 µm pore size
shipped in	ambient

C^o_{feed}	0.103	M
$C^o_{permeate}$	0	M
C_{feedd}	0.055	M
$C_{permeate}$	0.048	M

β	**2.25909**	$1/cm^2$
Diffusion Coefficient (l	**1.10E-05**	cm^2/sec
Flux	**6.15E-07**	mol/$(sec.cm^2)$

APPENDIX B

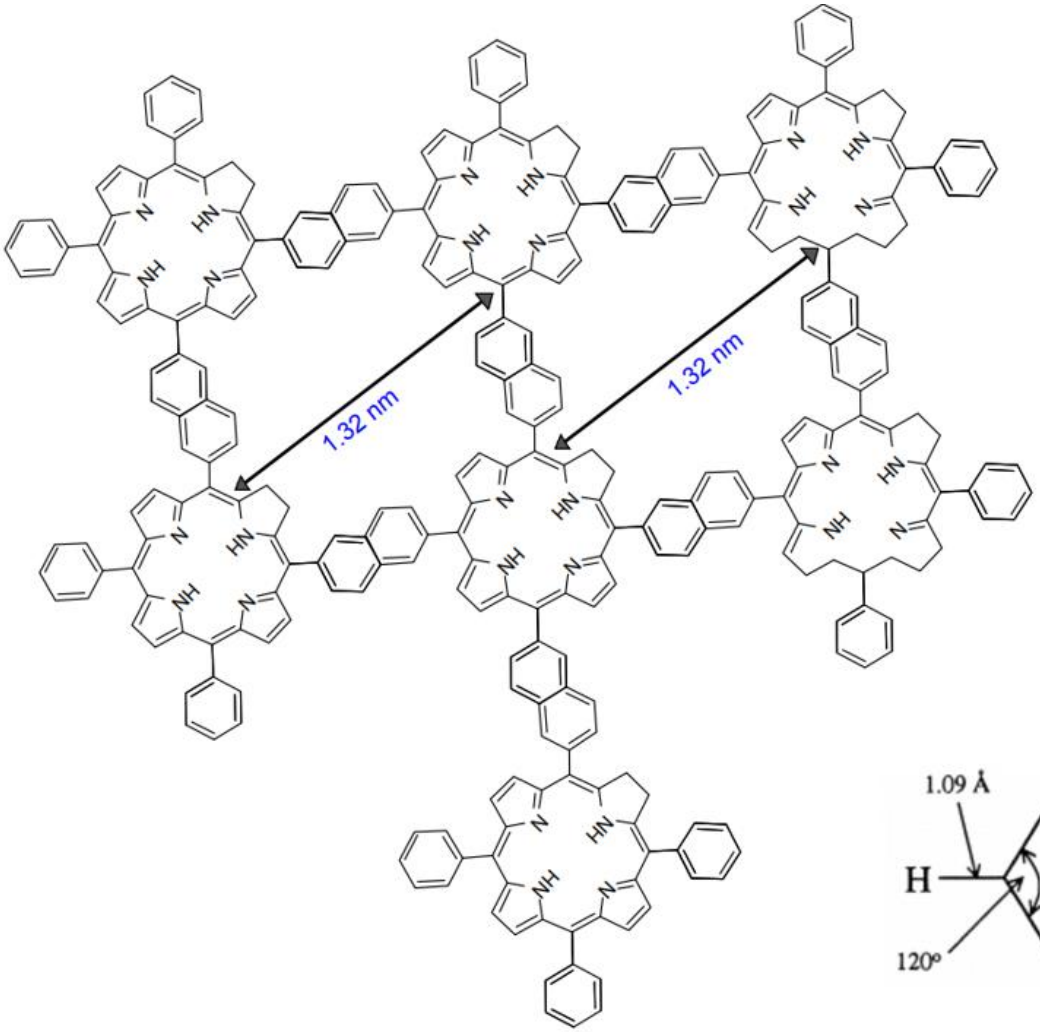

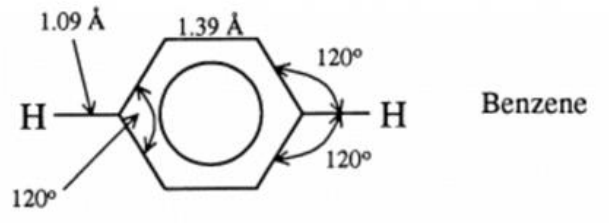

Benzene